1 potential, 2 potentials, 3 potentials–4: Untangling the UV photodissociation spectra of HI and DI

Robert J. Le Roy and Geoffrey T. Kraemer
Guelph-Waterloo Centre for Graduate Work in Chemistry and Biochemistry, University of Waterloo, Waterloo, Ontario N2L 3G1, Canada

Sergei Manzhos
Department of Chemistry, Queen's University, Kingston, Ontario K7L 3N6, Canada

(Received 7 June 2002; accepted 20 August 2002)

A comprehensive empirical analysis based on exact quantum simulations of all available total absorption coefficient and branching-ratio data for the UV photodissociation spectra of HI and DI has been used to determine the potential energy curves of the four excited electronic states $A\,^1\Pi_1$, $a\,^3\Pi_{0^+}$, $a\,^3\Pi_1$, and $t\,^3\Sigma_1^+$, and the associated transition moment functions. It is shown that there is no need to invoke coupling among the various final-state wave functions to explain the data.
© *2002 American Institute of Physics.* [DOI: 10.1063/1.1513303]

I. INTRODUCTION

The UV photochemical decomposition of HI has been studied for more than a century,[1] but it is still not fully understood. As shown in the top and bottom segments of Fig. 1, the low-energy portion of this spectrum consists of a broad peak (half-width ca. 6 000 cm^{-1}) centered near 45 000 cm^{-1}, known as the ''A-band.'' At higher frequencies the continuum intensity decreases by ca. 1/3 to a minimum around 53 300 cm^{-1}, and then grows monotonically into what is known as the ''B-band'' region, which merges with the discrete spectrum of transitions into highly excited $^3\Pi$ states at around 56 500 cm^{-1}. Research on this problem began in earnest in the 1930's with a series of measurements of the UV photodissociation continuum over an increasingly wide range of frequencies.[2–4] Rollefson and Booher suggested that the A-band spectrum might be due to transitions into two different final electronic states with asymptotes separated by the $I(^2P_{3/2}) \rightarrow I(^2P_{1/2})$ atomic spin orbit splitting,[2] but the available experimental data could not prove this, and in the first empirical inversion analysis applied to this system, Goodeve and Taylor[4] interpreted their spectrum in terms of transitions onto a single repulsive final state potential energy curve.

A decade later, Romand extended the range of the experimental data 10 000 cm^{-1} farther to the blue, spanning the B-band region where much of the absorption is due to unresolved discrete transitions into highly excited bound states.[5–7] This gave the first clear measure of the shape of the continuum at the onset of the B-band, although his absorption coefficients are ca. 20% smaller than those obtained in later work. His empirical analysis concluded that the lower-energy A-band continuum could not be explained by transitions to a single final electronic state, and his decomposition of that spectrum into two main components is roughly consistent with the present work, although Martin and Willard showed that his assignment of the final states was incorrect.[8] Twenty years later Huebert and Martin reported absorption coefficients for HI spanning most of the A-band and extending past the absorption minimum near 53 300 cm^{-1} into the low frequency edge of the B-band.[9] Within a scaling of 3.4% their results are consistent with the most recent measurements available for the A-band region. The current best total absorption coefficients for this system are the measurements for HI and DI on the interval 32 000–52 000 cm^{-1} reported by Ogilvie in 1971;[10] these are the key results on which all subsequent empirical analyses of this system (including the present work) have relied. The experimental total absorption coefficients used in the present analysis are plotted in the top and botton segments of Fig. 1.

By the early 1970's, photochemical studies had begun to be used to measure the relative intensities of photodissociation to yield $I(^2P_{3/2})$ versus $I^*(^2P_{1/2})$ atoms. In particular, from the absorption spectra of the atomic products produced by broadband flash photolysis, Donovan and Husain[11] concluded that ca. 1/5 of the atomic iodine produced was $I^*(^2P_{1/2})$. Studies of the kinetics of reactions of the translationally hot H atoms led to estimates of the quantum yield $\phi(I^*)$ of electronically excited iodine atoms at a handful of excitation energies.[12–15] However, while the one HI value of Cadman and Polanyi[12] and the four DI values of Betts[15] are consistent with results obtained by more direct methods (see below), others[11,13,14] are not.

The era of modern direct methods of determining quantum yields for this system began in 1975 when Clear *et al.*[16] used TOF photofragment translational spectroscopy to measure both $\phi(I^*)$ and the angular distributions of the $I(^2\Pi_{3/2})$ and $I^*(^2\Pi_{1/2})$ atoms produced by HI and DI photolysis at 266.2 nm. Since that time a variety of new methods were developed and applied to this system, including Doppler analysis of the product H atoms,[17–19] two-photon LIF of the atomic iodine,[20] monitoring of the infrared $I^*(^2P_{1/2}) \rightarrow I(^2P_{3/2})$ emission[21] and ion imaging,[22,23] as well as more TOF measurements of the fragment H atom intensities.[24] With a few exceptions, most of these measurements are fairly consistent with one another and with the results of the

 © 2002 American Institute of Physics

Downloaded 07 Nov 2002 to 129.97.80.195. Redistribution subject to AIP license or copyright, see http://ojps.aip.org/jcpo/jcpcr.jsp

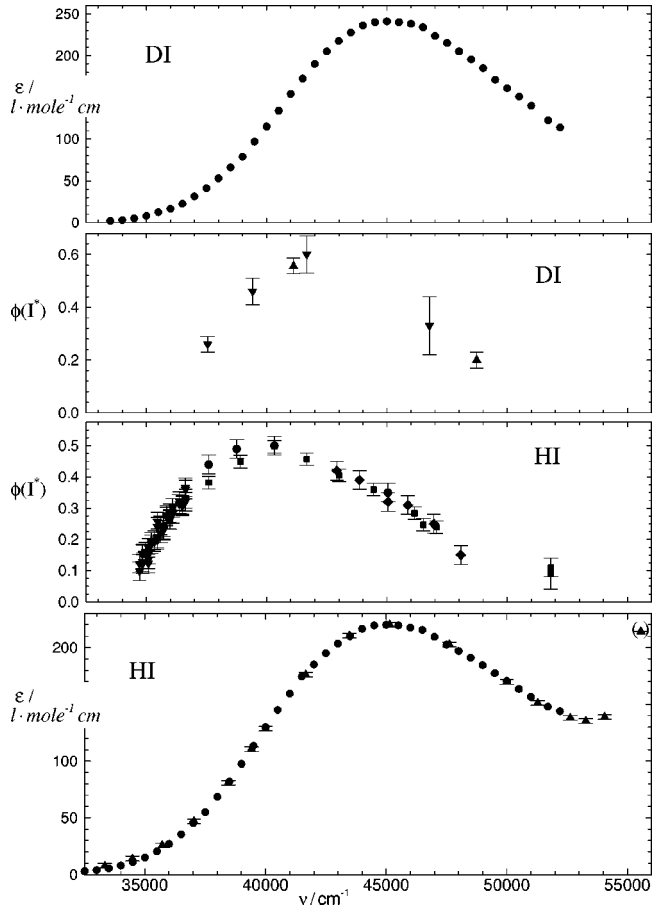

FIG. 1. Experimental data for the UV photodissociation of HI and DI. Round points in top and bottom segments are from Ogilvie (Ref. 10); triangular points with error bars in bottom segment are the data of Huebert & Martin (Ref. 9); ϕ(I*) for DI: gradient symbols are from Clear *et al.* (Ref. 16) and Betts (Ref. 15), and delta symbols the data of Heck and Chandler (Ref. 22); ϕ(I*) for HI: square points—Gendron and Hepburn (Ref. 26), round points—Regan *et al.* (Ref. 27), gradient symbols—Manzhos *et al.* (Ref. 28), and diamond symbols scaled (Ref. 27) Langford *et al.* (Ref. 25) data.

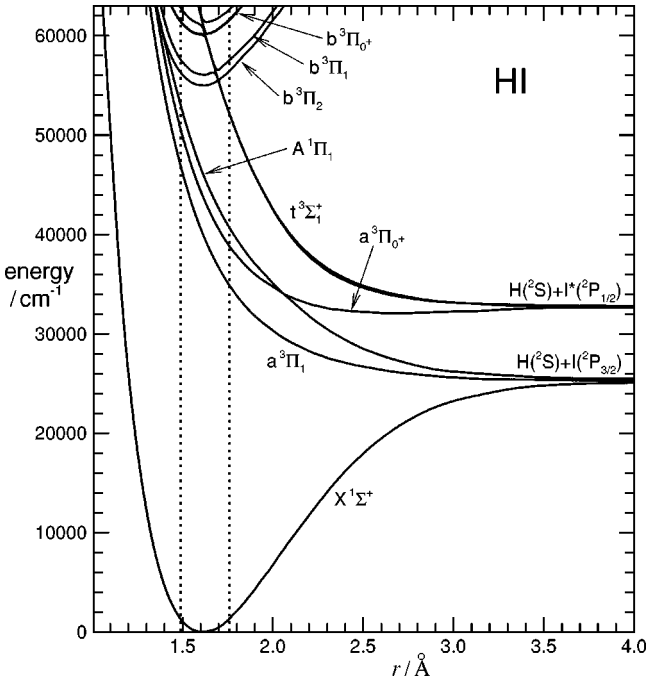

FIG. 2. *Ab initio* potentials for HI from Ref. 30.

present analysis, but they were only obtained at a scattered handful of photolysis frequencies.

By the late 1990's the sparse nature of and inconsistencies among the earlier HI photolysis quantum yield measurements stimulated five new sets of experiments. In 1995 Heck and Chandler[22] reported the first application of ion imaging techniques to this type of process, and presented ϕ(I*) values for DI at three frequencies. Then in 1998 both Langford *et al.*[25] and Gendron and Hepburn[26] reported quantum yields and product angular distributions at a number of wavelengths spanning most of the A-band region, the former using TOF analysis and the latter using Doppler spectroscopy of the H atom fragments. While these two studies agreed regarding the shape of the frequency dependence of ϕ(I*) and the anisotropy of the angular distributions, they disagreed sharply regarding the magnitude of the quantum yields. However, that discrepancy was settled the next year when Regan *et al.*[27] used REMPI detection of the I($^2P_{3/2}$) and I*($^2P_{1/2}$) fragments to obtain a set of quantum yields in good agreement with those of Gendron and Hepburn,[26] and showed that an experimental artifact had biased the Langford *et al.* detection of I*($^2P_{1/2}$) relative to I($^2P_{3/2}$). They also determined approximate wavelength-dependent corrections for the Langford *et al.* measurements. Finally, the most recent sets of results for this system are the dense set of quantum yield measurements on the low frequency side of the A-band obtained by ion imaging, reported in the preceding paper.[28] These results greatly improve the delineation of the frequency dependence of ϕ(I*) on the red side of the A-band, and agree closely with the one Regan *et al.*[27] measurement in this region. The two middle segments of Fig. 1 show the photolysis quantum yield data used in the present analysis.

While the theoretical work on this system has been less extensive, it has provided considerable insight. Although the data available at the time were quite limited, in 1937 Mulliken[29] published a remarkable study of this system whose essential predictions remain unchallenged to this day. He argued that the A-band portion of the UV continuum ($\nu \lesssim 50\,000$ cm^{-1}) was due to overlapping continuum transitions of increasing energy into the $a\,^3\Pi_1$, $a\,^3\Pi_{0^+}$, and $A\,^1\Pi_1$ states, the first and third of which dissociate to yield ground-state ($I^2P_{3/2}$), while the second yields I*($^2P_{1/2}$). However, he was unable to make firm predictions of their relative intensities. His discussion also allowed for contributions from transitions into the $t\,^3\Sigma_1^+$ state; however, in the region of good Franck-Condon overlap with the ground state, the t–state was predicted to lie at significantly higher energy than the others, and to contribute little to the A-band spectrum. Very recently Alekseyev *et al.*[30] reported very high quality *ab initio* calculations for this system which confirm most of the qualitative conclusions of Mulliken.[29] Their calculated potentials for the states relevant to this analysis are shown in Fig. 2; the vertical dotted lines drawn there indicate the locations of the inner and outer classical turning points for the $v=0$ level of HI, which are the approximate bound-

Downloaded 07 Nov 2002 to 129.97.80.195. Redistribution subject to AIP license or copyright, see http://ojps.aip.org/jcpo/jcpcr.jsp

aries of the Franck-Condon region sampled by the photodissociation data. A particularly interesting feature of these *ab initio* results was the determination of strong radial dependence in the transition moment functions driving the various electronic transitions; those results will be discussed in Sec. IV D.

Over the years there have been a number of efforts to analyze the UV photodissociation data for HI to empirically determine the upper-state potential curve (or curves) which give rise to it. In the earliest such inversion analysis, Goodeve and Taylor used a δ-function or Condon reflection method analysis[31,32] to interpret their data in terms of a single repulsive potential energy curve dissociating to ground state atoms.[4] Romand later concluded that the A-band spectrum could not be interpreted in terms of a single final-state potential, and used the reflection method to determine two final-state potentials.[7] On the other hand, Ogilvie's 1972 reflection method analysis of his A-band absorption coefficients concluded that they could be explained in terms of a single upper-state potential. However, the potentials he obtained for the HI and DI isotopomers were displaced from one another by ca. 500 cm^{-1}, a difference orders of magnitude larger than the isotopomer shifts one may expect to arise from Born-Oppenheimer breakdown effects. Moreover, the pointwise potentials he obtained show a troubling inflection point near 1.8 Å. In a subsequent analysis of those data based on quantum simulation of the photodissociation, Ogilvie and Tipping also claimed that a single final-state potential could explain more than 90% of the intensity.[33]

The first modern multistate analysis of this problem was that of Clear *et al.*,[16] who used the corrected δ–function approximation[34] to simulate and fit to Ogilvie's HI and DI absorption coefficients and the handful of (somewhat contradictory) quantum yield values available at the time. Their analysis determined (constant) transition moment functions and repulsive potentials represented by simple exponential functions for transitions into the three states Mulliken had predicted to be responsible for most of the A-band continuum: $a\,^3\Pi_1$, $a\,^3\Pi_{0^+}$, and $A\,^1\Pi_1$. However, they were unable to account for the HI absorption data for $\nu > 45\,500$ cm^{-1} and the DI data for $\nu > 47\,000$ cm^{-1} due to "... increasing participation of another absorption." A few years later van Veen *et al.*[24] reported conclusions about the anisotropy associated with the I* photolysis products which differed with those of most other work, and accompanied their measurements with a four-state analysis which placed the $t\,^3\Sigma_1^+$ potential function nearly coincident with that for $a\,^3\Pi_{0^+}$ in the Franck-Condon region, a result which sharply disagreed both with Mulliken's[29] predictions and with the recent *ab initio* potentials[30] shown in Fig. 2. The van Veen *et al.* results were the key input to a detailed coupled-states analysis by Levy and Shapiro, which again placed the $t\,^3\Sigma_1^+$ and $a\,^3\Pi_{0^+}$ state potentials very close to one another, and argued that this spectrum was strongly affected by coupling among the three $\Omega = 1$ final electronic states.[35] The results of the Levy-Shapiro work were four final-state potential functions, four transition moment strengths, and three interstate coupling strength functions. Finally, a decade later Gendron and Hepburn argued that the van Veen *et al.*[24] anisotropy measurements were simply not correct, and interpreted their new quantum yield measurements and Ogilvie's HI absorption coefficients in terms of a sum of potential energy curves for the $a\,^3\Pi_1$, $a\,^3\Pi_{0^+}$ and $A\,^1\Pi_1$ states. However, unlike Clear *et al.*, their analysis neglected the DI results, and it relied partially on spectral decomposition in a region beyond the range of any of their quantum yield measurements.

The preceding paragraphs summarizes the somewhat uncertain state of our understanding of this system at the onset of the present work. It leaves a number of open questions:

- The proposal of Levy and Shapiro[35] that coupling among the various final electronic states must be taken into account to describe the spectrum had been disputed,[26] but not really disproved.
- There was substantial disagreement between Gendron and Hepburn[26] and the initially reported Langford *et al.*[25] measurements regarding the magnitude of $\phi(I^*)$ near its maximum. While the results of Regan *et al.*[27] appear to have resolved this, further confirmation would be desirable.
- Since the 1948 Romand analysis,[7] no one had attempted to explain the composition of the spectrum extending into the B-band region up to the onset of the discrete spectrum at $56\,500$ cm^{-1},[36,37] even though the low-frequency tail of the B-band clearly overlaps the A-band.
- Most analyses had made little effort to take account of the HI and DI data together.
- The various estimates of the final-state potential functions were not in good agreement.
- The importance of the shape of the transition moment functions on these spectra has never been examined.

The present work addressed these concerns by undertaking a comprehensive empirical analysis of all available data for these systems in an effort to ascertain exactly how much information about the upper-state potential energy curves and the transitions moment functions giving rise to this spectrum could be determined from the available experimental data, and to determine the best possible estimates of those functions. This will provide quantitative tests of the recent *ab initio* calculations for this system,[30] and should allow us to make reliable predictions of the quantum yields as functions of frequency, for use in photochemical and hot-atom chemistry studies.

II. THEORY, MODELS AND COMPUTATIONAL METHODS

All of the present work was based on exact quantal calculations of the partial cross-section or continuum absorption coefficient for photodissociation from a thermal population of initial ground-state vibration-rotation levels into each of the relevant final electronic states. In the conventional units associated with the decadic molar absorption coefficient, l/mole·cm, the molar absorption coefficients for transitions into electronic state *s* are generated from the expression[38–40]

Downloaded 07 Nov 2002 to 129.97.80.195. Redistribution subject to AIP license or copyright, see http://ojps.aip.org/jcpo/jcpcr.jsp

$$\epsilon(\nu,\mathrm{T};s)=\frac{10^{-19}N_{\mathrm{A}}}{\ln(10)}\frac{8\pi^3\nu}{3hc}g_s\sum_v\sum_J F_{v,J}(\mathrm{T}) \times\sum_{J'}\frac{S_J^{J'}}{2J+1}|\langle\psi_{E,J'}(r)|M_s(r)|\psi_{v,J}(r)\rangle|^2. \tag{1}$$

Here, N_{A} is Avogadro's number, ν is the wave number of the light (in cm^{-1}), g_s the upper-state electronic degeneracy,[41] $F_{v,J}(\mathrm{T})$ the fractional thermal population of initial-state vibration–rotation level (v,J), J' the final (continuum) level angular momentum quantum number, and $S_J^{J'}$ the Hönl-London rotational intensity factor.[42]

The initial-state radial wave function $\psi_{v,J}(R)$ at energy $E_0(v,J)$ and the final-state continuum wave function $\psi_{E,J'}(R)$ at energy $E=E_0(v,J)+h\nu$ are obtained by exact numerical solution of the radial Schrödinger equation

$$-\frac{\hbar^2}{2\mu}\frac{d^2\psi(r)}{dr^2}+\left\{V(r)+\frac{[J(J+1)-\Omega^2]\hbar^2}{2\mu r^2}\right\}\psi(r) =E\psi(r) \tag{2}$$

for the relevant initial- or final-state potential energy function $V(r)$, where μ is the reduced mass of the two atoms forming the molecule and Ω the projection of the total electronic angular momentum on the molecular axis. The mesh and range parameters governing the numerical integration of Eq. (2) and the asymptotic amplitude convergence criterion for the continuum wave functions were chosen to ensure that calculated intensities were accurate to better than 10^{-5} of the intensity maximum, which is ca. 10^{-3} smaller than typical experimental uncertainties.

Since HI and DI have relatively large vibrational and rotational level spacings, and all of the available experimental data were obtained at modest to low temperatures, the summations over v and J in Eq. (1) could readily be performed; this involves only $v=0$ and 1 and $J\leqslant 18$ for HI and $J\leqslant 25$ for DI.

The experimental data considered herein consist of both total absorption coefficients

$$\epsilon_{\mathrm{tot}}(\nu;\mathrm{T})=\sum_s\epsilon(\nu,\mathrm{T};s) \tag{3}$$

and the quantum yields $\phi(\mathrm{I}^*)$ for electronically excited product iodine atoms:

$$\phi(\mathrm{I}^*)=\{\epsilon(\nu,\mathrm{T};a\,^3\Pi_{0^+})+\epsilon(\nu,\mathrm{T};t\,^3\Sigma_1^+)\}/\epsilon_{\mathrm{tot}}(\nu;\mathrm{T}), \tag{4}$$

where $s=a\,^3\Pi_{0^+}$ and $t\,^3\Sigma_1^+$ are the electronic states which correlate with production of electronically excited $\mathrm{I}^*(^2P_{1/2})$ atoms.[29] These observables are readily generated from linear combinations of the partial absorption coefficients of Eq. (1) calculated for the participating excited electronic states. One other type of observable reported for this system is the anisotropy of the photofragment distribution, which effectively determines the fraction of molecules which photodissociate to a given asymptote through $\Omega=1$ ($A\,^1\Pi_1$ or $a\,^3\Pi_1$ or $t\,^3\Sigma_1^+$) versus $\Omega=0$ ($a\,^3\Pi_{0^+}$) states. However, rather than utilize them in the analysis, these results will be used as an independent check on the results of our analysis.

A. The initial-state potential energy function

The ground electronic state potential energy functions for HI and DI are very well known. In particular, Coxon and Hajigeorgiou use a combined analysis of high resolution spectroscopic data for both isotopomers to determine explicit analytic functions for them based on a generalized Morse potential form in which the exponent coefficient is allowed to be a function of the internuclear distance.[43] Their analysis also incorporates Born-Oppenheimer breakdown correction functions which give rise both to small differences between the effective intermolecular potentials for the two isotopomers, and to a weak distance-dependence of the reduced mass associated with the centrifugal potential energy term in Eq. (2). These are the potential energy functions for the ground electronic states of HI and DI used in the present work. Although these analytical potentials are known to behave badly at distances beyond 3 Å ,[44] that occurs far beyond the range of the initial-state wave functions involved in this analysis, and hence has no effect on our calculations.

B. The final-state potential energy functions

Two different types of functional forms were considered for the potential energy functions of the (mainly) repulsive electronically excited final states associated with the photodissociation process. The first is an exponential function with the exponent coefficient expanded as a power series in a chosen radial distance variable

$$V_{\mathrm{exp}}(r)=\mathfrak{D}_s+A_s\,e^{-\beta(y_{\mathrm{p}})\cdot(r-r_{\mathrm{x}})}, \tag{5}$$

where $\mathfrak{D}_s$ is the energy at the asymptote of electronic state s, r_{x} is a chosen fixed reference distance,

$$\beta(y_{\mathrm{p}})=\beta_0+\beta_1 y_{\mathrm{p}}+\beta_2 y_{\mathrm{p}}{}^2+\ldots \tag{6}$$

and $y_{\mathrm{p}}\equiv(r^{\mathrm{p}}-r_{\mathrm{x}}{}^{\mathrm{p}})/(r^{\mathrm{p}}+r_{\mathrm{x}}{}^{\mathrm{p}})$, where p is a small positive integer. The reference distance r_{x} is most conveniently chosen to lie at the middle of the Franck-Condon overlap region, near the initial-state equilibrium distance, in which case the quantity $[\mathfrak{D}_s+A_s]$ will be the vertical excitation energy onto this potential in the middle of the Franck-Condon overlap region.

A second type of potential form was introduced to allow for a case in which the final-state potential had an attractive well. The form used for this case is a modified version of the ''extended Morse oscillator'' or EMO function of Ref. (45),

$$V_{\mathrm{EMO}}=[\mathfrak{D}_s-\mathfrak{D}_e]+\mathfrak{D}_e[e^{-\beta(y_{\mathrm{p}})\cdot(r-r_e)}-1]^2, \tag{7}$$

where $\mathfrak{D}_e$ and r_e, respectively, are the well depth and equilibrium distance at the potential minimum, and $\mathfrak{D}_s$, $\beta(y_{\mathrm{p}})$ and y_{p} are defined as above. This expression differs from the basic EMO form of Ref. 45 in that the distance-dependent exponent coefficient $\beta(y_{\mathrm{p}})$ is expanded about the reference distance r_{x} (the middle of the Franck-Condon overlap region) rather than about the potential minimum position r_e. This definition minimizes the correlation between parameters governing the vertical energy and the shape of the repulsive

Downloaded 07 Nov 2002 to 129.97.80.195. Redistribution subject to AIP license or copyright, see http://ojps.aip.org/jcpo/jcpcr.jsp

potential wall in the Franck-Condon overlap region, so this parameterization is particularly appropriate when the the existence and approximate position of the potential well are important, but the details of its shape are not. In contrast, for cases in which the Franck-Condon overlap region extends into the attractive well of the final-state potential, another approach should be used.[38,46–48]

Since the Franck-Condon overlap region, the domain over which the radial wave functions of the thermally populated initial-state levels has significant amplitude, is fairly narrow for this system (ca. 1.49−1.76 Å), the photodissociation data will be only modestly sensitive to features of these potentials other than their energy and slope in the interaction region. Thus, we expect to require at most a low-order polynomial expansion to describe $\beta(y_p)$ in these potential forms.

C. The transition moment functions

The models for the transition moment functions used herein are either a power series expansion in a chosen radial variable,

$$M_s(r)=\sum_{i=0} c_i y_p^{\,i}, \tag{8}$$

with y_p defined as above, or a constant factor multiplying a known function, $M_s(r)=c_0\mathbb{M}_s(r)$, where $\mathbb{M}_s(r)$ is a known function determined (say) from electronic structure calculations, and c_0 is a scaling factor to be determined from the analysis.

D. The least-squares fitting procedure

The present analysis uses nonlinear least-squares fits to experimental data to determine optimum values of parameters characterizing the various final-state potential energy and transition moment functions. In these fits, all data are considered simultaneously, each weighted by the inverse-square of its estimated uncertainty (see below). The quality of fit is characterized by values of the dimensionless root mean square residual or RMSR,

$$\mathrm{RMSR}=\left\{(1/N_d)\sum_{i=1}^{N_d}\left[(Y_{\mathrm{calc}}(i)-Y_{\mathrm{obs}}(i))/u(i)\right]^2\right\}^{1/2}, \tag{9}$$

where each of the N_d experimental data $Y_{\mathrm{obs}}(i)$ has uncertainty $u(i)$ associated with it, and $Y_{\mathrm{calc}}(i)$ is the value of datum-i calculated from the model. While nonlinear fits require initial trial values of the parameters defining the model being treated, simple reflection or δ-function approximation arguments[32,42] and the final-state potentials of Mulliken[29] or Alekseyev *et al.*[30] yield sufficiently plausible potential parameter estimates that least-squares stability was not a serious problem.

An essential requirement of any least-squares procedure is the ability to generate values of the partial derivatives of each datum with respect to each of the parameters of the model. Consideration of Eq. (1) shows that partial derivatives with respect to the parameters defining the transition moment functions can be evaluated exactly from matrix elements of partial derivatives of the transition moment functions, $\langle\psi_{E,J'}(r)|\partial M_s(r)/\partial p_j|\psi_{v,J}(r)\rangle$. These matrix elements may be computed from the bound and continuum wave functions at the same time as the transition intensities themselves, and hence are obtained with very little additional computational effort. However, an analogous direct way of calculating exact partial derivatives of the individual partial absorption coefficients sections with respect to the parameters defining the final-state potentials has not yet been fully developed. Thus, the latter were evaluated by symmetric finite differences, where the parameter increment was chosen by an algorithm which ensures that on average (across the entire data set), the difference in the observables was less than 0.1 times their experimental uncertainty. All of the calculations reported herein were performed using program BCONT.[46] One of the key features of this code is its ability to simultaneously fit to data for multiple isotopomers and treat quantum yield or branching ratio data together with total or partial absorption coefficient measurements.

III. DATA USED IN THE ANALYSIS

In any least-squares treatment of data, the set of uncertainties (or weights) associated with different measurements has the ability to significantly skew the results. It is therefore important to record the choices made in this regard. An overview of the data used in the present analysis is presented in Table I. The total absorption coefficients for HI and DI measured by Oglivie[10] are the most important of these, since they span the entire A-band and extend into the B-band region with a fairly dense and internally consistent set of measurements. It is these data which determine the absolute magnitudes of the transition moment functions. Moreover, the significant differences between the profiles of the initial-state $v=0$ radial wave function for these two isotopomers, combined with the fact that any valid model must simultaneously account for both sets of observations, makes the simultaneous treatment of both sets of data a particularly demanding feature of the present analysis.

Ogilvie's paper stated that his absorption coefficients had an absolute uncertainty of $\pm 5\%$ and a relative accuracy of $\pm 2\%$, "except at the extremes of the range of absorption" where the relative uncertainties are (presumably) larger.[10] His $\pm 5\%$ reflects his uncertainties regarding the absolute pressure measurements determining the HI or DI concentration in the absorption cell. However, the only effect of an error of this type on an empirical analysis would be to introduce a common multiplicative correction factor scaling the magnitude of all the transition moment functions being determined. On the other hand, if the error in the DI pressure measurement differed from that for HI, it would introduce an artificial apparent inconsistency between these two data sets. In the present analysis, therefore, Ogilvie's HI pressure measurements are taken to be exact, while the global scaling factor f_ϵ(DI) for his DI absorption coefficients is treated as a parameter to be determined in the least-squares fit procedure. However, Ogilvie's 5% absolute (pressure measurement) uncertainty associates an overall multiplicative uncertainty of $\pm 2.5\%$ with the strength of any transition moment functions determined from his data.

Downloaded 07 Nov 2002 to 129.97.80.195. Redistribution subject to AIP license or copyright, see http://ojps.aip.org/jcpo/jcpcr.jsp

TABLE I. Experimental data used in the present empirical analysis of the UV photodissociation spectra of HI and DI. Values and uncertainties in $\epsilon_{tot}(\nu,T)$ have units l/mole cm, while those for $\phi(I^*)$ are dimensionless.

Property	Species	T/K	N_d	Range [cm^{-1}]	Uncertainty	Source
$\epsilon_{tot}(\nu,T)$	HI	294	41	32 500–52 200	1–2	Ogilvie (Ref. 10)
$\epsilon_{tot}(\nu,T)$	DI	294	38	33 500–52 200	1–2	Ogilvie (Ref. 10)
$\epsilon_{tot}(\nu,T)$	HI	296	12	33 333–50 000	2	Huebert and Martin[a]
$\epsilon_{tot}(\nu,T)$	HI	195	5	50 000–55 555	2	Huebert and Martin[a]
$\phi(I^*)$	DI	205	3	39 420–46 770	0.05–0.11	Betts (Ref. 15)
$\phi(I^*)$	DI	205	1	37 550	0.03	Clear *et al.* (Ref. 16)
$\phi(I^*)$	HI	10	1	51 813	0.09	van Veen *et al.* (Ref. 24)
$\phi(I^*)$	HI	291	1	51 813	0.05	Wight and Leone (Ref. 21)
$\phi(I^*)$	DI	10	3	32 489–48 733	0.03	Heck and Chandler (Ref. 22)
$\phi(I^*)$	HI	10	9	37 593–48 780	0.02	Gendron and Hepburn (Ref. 26)
$\phi(I^*)$	HI	10	6	42 918–48 076	0.02	Langford[b]
$\phi(I^*)$	HI	10	5	35 714–45 045	0.03	Regan *et al.* (Ref. 27)
$\phi(I^*)$	HI	10	39	34 722–36 630	0.03	Manzhos *et al.* (Ref. 28)

[a]Data (Ref. 9) scaled by a factor of 1/0.967 to give consistency with Ogilvie's measurements for $185 \leqslant \lambda \leqslant 200$ nm.
[b]Data of Langford *et al.* (Ref. 25) for $\lambda \leqslant 233$ nm, as corrected by Regan *et al.* (Ref. 27).

The question of the relative uncertainty—what uncertainty to associate with the individual HI absorption coefficients—is a more difficult one to address. Both the smoothness of Ogilvie's measurements and the results of our analysis suggests that the relative uncertainties in the larger absorption coefficient values are much smaller than the 2% mentioned in his paper. After considerable experimentation, we decided to weight each of his data by an uncertainty of ± 1 [l/mole cm]. This would correspond to Ogilvie's 2% for $\epsilon_{tot}=50$ [l/mole cm], but would be smaller than that for larger values, and larger for smaller values. The latter consideration takes account of Ogilvie's expectation that the relative uncertainties are larger ''at the extremes of the range of absorption,'' as far as the red end of the spectrum (where the absorption coefficients approach zero) is concerned. To include an analogous allowance at the blue end of his data range, we chose to double the uncertainties associated with his (two for each of HI and DI) data points for $\nu > 51\,000$ cm^{-1} to 2 [l/mole cm].

The other total absorption coefficient data used in the present analysis are those Huebert and Martin,[9] who obtained 11 values on the interval $33\,333-50\,000$ cm^{-1} for HI at 296 K, and 6 values at frequencies $50\,000-55\,555$ cm^{-1} for HI at 195 K. Comparisons of the former with the more extensive results of Ogilvie allowed us to determine a scaling factor of $1.034(\pm 0.007)$ to account for inconsistency between the pressure measurements in the two experiments, and also led us to attribute uncertainties of ± 2 [l/mole cm] to these data. Moreover, their datum farthest to the blue (at 180 nm, in parentheses in Fig. 1) is believed to be compro-

TABLE II. Results of fitting one or two potentials to Ogilvie's (Ref. 10) data, using constant transition moment functions.

	Potential energy function(s) used				$V_s(r_x)/cm^{-1}$	
Species	No.	How obtained	$\beta(y_p)$	RMSR	$s=A\,^1\Pi_1$	$a\,^3\Pi_{0^+}$
HI	1	fit to HI data alone	constant	4.34	47 258 (± 92)	—
DI	1	fit to DI data alone	constant	2.99	46 618 (± 42)	—
HI	1	from fit to DI data	constant	11.81	46 618	—
DI	1	from fit to HI data	constant	14.34	47 258	—
HI	1	fit to HI data alone	linear[a]	1.99	48 025 (± 130)	—
DI	1	fit to DI data alone	linear[a]	1.81	46 841 (± 48)	—
HI	1	from fit to DI data	linear[a]	12.29	46 841	—
DI	1	from fit to HI data	linear[a]	16.68	48 025	—
HI & DI	1	fit to HI & DI data	constant	7.17	46 838 (± 80)	—
HI & DI	1	fit to HI & DI data	linear[a]	6.98	46 988 (± 140)	—
HI	2	fit to HI data alone	constant	0.84	50 678 (± 1500)	45 688 (± 840)
DI	2	fit to DI data alone	constant	0.84	47 307 (± 230)	44 687 (± 590)
HI	2	from fit to DI data	constant	11.68	47 307	44 687
DI	2	from fit to HI data	constant	15.34	50 678	45 688
HI & DI	2	fit to HI & DI data	constant	6.52	47 608 (± 1000)	44 231 (± 3200)
HI	2	fit to HI data alone[d]	constant	0.84	45 050 (± 280)	55 881 (± 4200)
DI	2	fit to DI data alone[d]	constant	1.03	46 208 (± 83)	53 061 (± 850)
HI & DI	2	fit to HI & DI data[d]	constant	2.51	45 730 (± 170)	76 781 ($\pm 29\,000$)

[a]A linear function of the expansion variable $y_3(r)=(r^3-r_x^3)/(r^3+r_x^3)$.
[b]With the transition moment strength ratio fixed from the DI fit.
[c]With the transition moment strength ratio fixed from the HI fit.
[d]Initial trial parameters chosen so that the fitted $a\,^3\Pi_{0^+}$ potential will lie above that for $A\,^1\Pi_1$ in the Franck-Condon overlap region.

Downloaded 07 Nov 2002 to 129.97.80.195. Redistribution subject to AIP license or copyright, see http://ojps.aip.org/jcpo/jcpcr.jsp

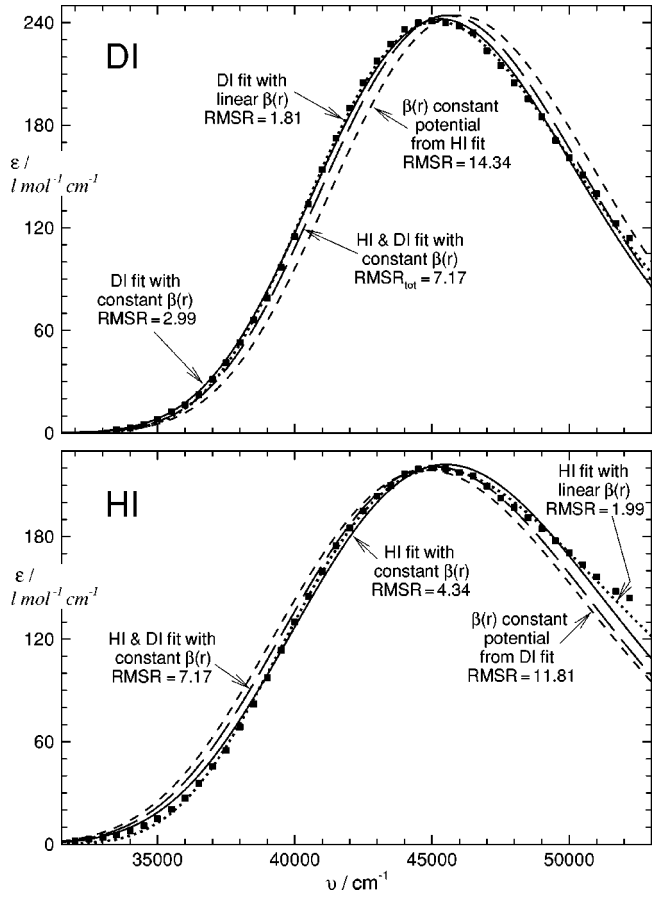

FIG. 3. Results of 1-potential fits to Ogilvie's (Ref. 10) total absorption coefficients (square points).

mised by overlap with the onset of the discrete band spectrum, so it was omitted from the analysis.

The uncertainties used for the quantum yield data were those reported in the literature, with minor modifications. In particular, while the uncertainties Gendron and Hepburn reported for their nine measurements varied from 0.006 to 0.018, the irregularities in their frequency dependence and the degree of consistency with the results of other work led us to weight them all with uncertainties of ± 0.02. Since no uncertainties were reported for the three DI values of Heck and Chandler,[22] we assigned them uncertainties of 0.03, based on those reported for the analogous ion-imaging results of Ref. (28). In addition, while the results reported by Langford *et al.*[25] were later shown to be somewhat in error,[26,27] the values obtained on applying frequency-dependent correction factors determined by Regan *et al.*[27] were in good agreement with other data on the blue side of the A-band, and since they extend to somewhat higher frequency than most other results, their six highest-frequency quantum efficiencies $\phi(\mathrm{I}^*)$ were used in our analysis with the reported uncertainties of ± 0.03. The lower-frequency Regan-corrected[27] Langford *et al.*[25] data were omitted, since the discrepancies with other measurements was somewhat larger, and the scaling correction was in any case only approximate. Finally, although the anisotropy measurements of van Veen *et al.*[24] are contradicted by all other work, their quantum yields at their three experimental wavelengths are consistent with those obtained by others. However, since the uncertainties reported for their two longer wavelength values are larger than those for later work, only their $\phi(\mathrm{I}^*)$ value for 193 nm was utilized in the present analysis.

IV. RESULTS

A. Analysis in term of one final-state potential

Since much of the earlier work on this problem interpreted the then-available data in terms of transitions into only one or two final electronic states, we begin by examining the question of whether, within their uncertainties, the total absorption coefficient data could in fact be fully explained in this way. To this end, the results of a number of one-potential fits to Ogilvie's HI and DI absorption coefficients,[10] considered both separately and together, are summarized in Table II and Fig. 3. It would be tedious and unnecessary to list all of the potential energy and transition moment function parameters defining the various models considered in the course of the present work. However, to facilitate comparison among the various models, Table II lists the values of the final-state potential energy function(s) at the expansion center $r_x = 1.609$ Å, which lies approximately at the minimum of the ground-state HI potential energy curve. These potential energies are expressed relative to the energy at the minimum of the ground-state potential; for the exponential potential form of Eq. (5), $V_s(r_x) = \mathfrak{D}_s + A_s$.

We first consider fits to a single final-state potential energy curve which is represented by the exponential function of Eq. (5) and has the same asymptote as the ground-state potential, $\mathfrak{D}_s = \mathfrak{D}_e(X) = 25\,778$ cm^{-1},[43] with the transition moment function being treated as a constant (independent of r). The first two rows of Table II and the solid curves in Fig. 3 show the results of independent fits of the HI and the DI data sets with the potential function exponent parameter treated as a constant, $\beta(y_p) = \beta_0$. The quality of fit is clearly poor for both isotopomers, with average discrepancies of 3–4 times the experimental uncertainties. Moreover the potentials obtained are quite inconsistent with one another, with that for HI lying more than 600 cm^{-1} above the one for DI. This inconsistency is further demonstrated by the third and fourth rows of the table and the short-dash curves in Fig. 3, which show the very much worse quality of the predictions (RMSR = 11.8 or 14.3) for the other isotopomer, as generated from the potentials yielded by the single-isotopomer fits of the first two rows of this table.

In an effort to improve on the above results, we also performed further single-isotopomer fits to the HI and DI absorption coefficients while allowing the exponent parameter $\beta(y_p)$ to vary with distance. The results of those fits are shown as dotted curves in Fig. 3 and in rows 5–8 of Table II. With the RMSR's for the HI and DI fits now reduced to 2.0 and 1.8, respectively, it is clear that use of this more flexible model potential greatly improves the quality of fit. However, the incompatibility of the potentials obtained from these single-isotopomer fits is substantially increased, with the DI-fit potential at $r = r_x$ now lying almost 1200 cm^{-1} below that for HI, and the ability of the potential obtained

Downloaded 07 Nov 2002 to 129.97.80.195. Redistribution subject to AIP license or copyright, see http://ojps.aip.org/jcpo/jcpcr.jsp

from one isotopomer to predict the data for the other is even worse than before.

As a final test of one-potential models, a fit to the data for both isotopomers simultaneously was performed using each of the above potential models [constant versus linear $\beta(y_p)$]; the results are summarized in rows 9 and 10 of Table II, and shown as long-dash curves in Fig. 3. The large RMSR values and the systematic discrepancies seen in the figure further confirm the fact that within a model which attempts to attribute the absorption to transitions into a single final electronic state, the data for the two isotopomers are completely inconsistent. Thus, it is clear that more than one final electronic state is necessary to explain these data. It is also clear that the availability of data of equivalent quality for the two isotopomers is a key discriminating feature of this analysis.

A final point here is the fact that allowing the transition moment to vary with distance had no effect on the above results and conclusions. In particular, allowing $M_s(r)$ to be a linear function with a large positive or negative slope at r_x gave rise to a shift of the potential energy parameter $A_s = V_s(r_x)$, but it had essentially no effect on the quality of the fit. As discussed in Ref. (38), this insensitivity to the shape of the transition moment function(s) is to be expected for cases in which most of the absorption arises from the $v=0$ level of the initial electronic state.

B. Analysis in terms of two final-state potentials

Figure 4 and the last eight rows of Table II illustrate the results of fits to a model which treats the absorption as being due to transitions into two different final electronic states, one sharing the same asymptote as the ground electronic state, and one which dissociates to yield H+I* at an asymptote some 7603.15 cm^{-1} above the former. For convenience, these two potentials are given the labels of electronic states known to dissociate to these two limits.

The first two two-potential cases (rows 11 and 12 in Table II and solid curves in Fig. 4) show that for either isotopomer considered separately, a model which attributes the absorption to two final-state potential energy functions does provide an entirely satisfactory description of the data, in that the associated RMSR values for both cases are less than unity. Indeed, the size of these RMSR values is taken as confirmation of the validity of our assumptions regarding the relative uncertainties associated with the Ogilvie data (see Sec. III). However, the differences among the results in the next three rows of the table and between the long- and short-dash curves in Fig. 4 again indicate that within a model which allows for only two final electronic states, the HI and DI absorption coefficients are completely incompatible with one another.

Since the energies ($\mathfrak{D}_s$) at the asymptotes of these potentials are substantially smaller than their values in the Franck-Condon overlap region ($\approx \mathfrak{D}_s + A_s$), one might expect that an analysis of this type would not be particularly sensitive to the locations of those asymptotes. Moreover, the results of any nonlinear least-squares fit may depend on the initial trial values chosen for the various parameters of the model. Thus, it seemed possible that the result that the potential with the lower asymptote ($A\,^1\Pi_1$) lay above the other one in the Franck-Condon region could be an artifact due to a memory of those initial trial values, rather than being a sound physical conclusion yielded by the data. The above two-potential fits were therefore repeated using initial trial parameters which placed the $A\,^1\Pi_1$ potential (the one with the lower asymptote) below the $a\,^3\Pi_{0^+}$ curve in the Franck-Condon region.

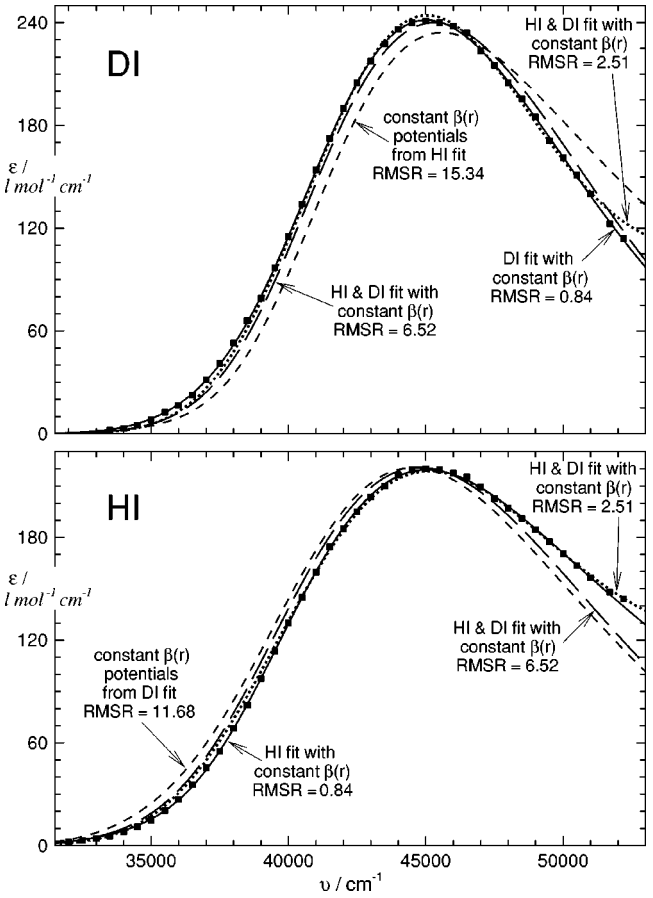

FIG. 4. Results of 2-potential fits to Ogilvie's (Ref. 10) total absorption coefficients (square points).

As is shown by the last three rows of Table II, this approach did yield fitted potentials with the reverse energy ordering at $r=r_x$, and the single-isotopomer fits again fully explain the data within their uncertainties. However, the values of $V_s(r_x)$ for those separate HI and DI fits are again quite incompatible. Although the large parameter uncertainties associated with these fits leaves room for doubt regarding the rigor of this last conclusion, the combined-isotopomer fit of the last row of the table still has an RMSR value of 2.5, which is three times as large as that for the single-isotopomer two-potential fits, which we take to define the resolution of these data. Moreover, giving the exponent functions $\beta(y_p)$ a strong dependence on distance did not significantly improve the quality of fit or reduce the parameter uncertainties. Thus, it seems clear that the total absorption coefficients cannot be properly explained by a model which allows for transitions into only two final electronic states. Once again, however, it is clear that the existence of good data for the two isotopomers was essential for reaching physically-significant con-

Downloaded 07 Nov 2002 to 129.97.80.195. Redistribution subject to AIP license or copyright, see http://ojps.aip.org/jcpo/jcpcr.jsp

clusions regarding the validity of a two-final-state model.

As a final test of the validity of a two-potential analysis, the potential energy and transition moment functions of our two combined-isotopomer two-potential fits (rows 15 and 18 in Table II), were used to predict the quantum yield data for HI and DI listed in Table I. On average, the predictions of these two-potential models disagreed with experiment by, respectively, 9.1 and 7.0 times the experimental uncertainties. Moreover, even when the quantum yield data were also used (together with the HI and DI absorption coefficients) as data in the fit, the lowest overall RMSR value obtained was 5.4. Thus, it is clear that use of only two final-state potential energy functions will not explain the experimental data for this system.

C. Analysis in terms of three final-state potentials

The course of this work included numerous fits to the combined absorption coefficient and quantum yield data sets using three final-state potential curves. However, a detailed presentation of those results would add considerable clutter to this paper, while yielding limited additional physical insight, so we content ourselves with a summary of the conclusions reached.

The preceding sections clearly demonstrated that even if the quantum efficiency $\phi(\mathrm{I}^*)$ data are neglected, the HI and DI total absorption coefficients alone cannot be represented adequately by only two final-state potentials. The early work of Clear *et al.*[16] had shown that a three-potential analysis could account for both the absorption coefficients for the two isotopomers and the limited amount of branching ratio data available at the time. This conclusion was reaffirmed by the analysis of Gendron and Hepburn;[26] however, while the $\phi(\mathrm{I}^*)$ data they used were more extensive and more reliable, their neglect of the available DI data makes the rigor of their conclusions somewhat uncertain. In any case, the present work did confirm the conclusion that across much of the A-band region, the HI and DI total absorption coefficient and quantum efficiency data may be reasonably well accounted for by fits to three final-state potentials, two of which dissociate to ground-state atoms while the third dissociates to yield $\mathrm{I}^*(^2P_{1/2})$ atoms. However, as was found by Clear *et al.*,[16] this analysis becomes increasingly unsatisfactory at transition frequencies significantly higher than those associated with the A-band absorption intensity maxima.

D. Analysis in terms of four final-state potentials

All of the results presented in this section are based on simultaneous fits to all of the 164 absorption coefficient and quantum efficiency data for HI and DI listed in Table I. The four final-state potentials are identified as suggested by Mulliken,[29] with the $A\,^1\Pi_1$ and $a\,^3\Pi_1$ states dissociating to yield H or D plus a ground state $\mathrm{I}(^2P_{3/2})$ atom, and the $a\,^3\Pi_{0^+}$ and $t\,^3\Sigma_1^+$ states dissociating to yield H or D plus $\mathrm{I}^*(^2P_{1/2})$. Using the ground-state dissociation energy from Ref. 43, this means that the potentials for the first two of these states have their asymptote at energy $\mathfrak{D}_s=\mathfrak{D}_e(X)=25\,778\ \mathrm{cm}^{-1}$, while for the other two $\mathfrak{D}_s=\mathfrak{D}_e(X)+7603=33\,381\ \mathrm{cm}^{-1}$. Following the transition moment strength convention of Whiting *et al.*,[41] the electronic degeneracy factors used in the calculations were $g_s=2$, 1, 2, and 2, respectively, for the $A\,^1\Pi_1$, $a\,^3\Pi_{0^+}$, $a\,^3\Pi_1$, and $t\,^3\Sigma_1^+$ states.

In all previous empirical analyses of these data sets, all final-state potential energy curves were represented by the exponential function of Eq. (5) with the exponent coefficient treated as a constant $[\beta(y_\mathrm{p})=\beta_0]$. In spite of the narrowness of the Franck-Condon overlap region (ca. 1.49−1.76 Å), this was inadequate here, and obtaining optimum agreement with experiment required the exponent coefficient for two of the potentials to be functions of the expansion variable $y_\mathrm{p}(r)=(r^\mathrm{p}-r_\mathrm{x}^\mathrm{p})/(r^\mathrm{p}+r_\mathrm{x}^\mathrm{p})$. While a range of values of p were considered, $\mathrm{p}=8$ was chosen for our final fits because of the desirable extrapolation properties of the resulting $y_8(r)$ expansion variable.[49,50] Moreover, since the *ab initio* results of Ref. 30 indicate that the $a\,^3\Pi_{0^+}$ state potential has a well of depth ca. 600 cm^{-1} with its minimum located at 2.7 Å, fits were also performed using the EMO potential form of Eq. (7) for this state. In the following discussion, therefore, the $a\,^3\Pi_{0^+}$ state potential is identified as having either the exponential ("exp") or the EMO form, and the potential exponent coefficients are either held constant $(\beta(y_8)=\beta_0)$ or allowed to be linear or quadratic $(\beta(y_8)=\beta_0+\beta_1 y_8(r)+\cdots)$. In practice, the data are most strongly sensitive to the details of the transitions into the $A\,^1\Pi_1$ and $a\,^3\Pi_{0^+}$ states, so efforts to determine additional potential function shape parameters (β_1 and β_2 values) focussed on those two states, and the potentials for the other two states were always treated as simple exponential functions with constant exponent coefficients $\beta(y_\mathrm{p})=\beta_0$.

In all of the fits reported below, the transition moment expansion coefficients $\{c_i(s)\}$, the exponent expansion parameters $\{\beta_0(s)\}$ (and sometimes also $\{\beta_1(s)\}$ and $\{\beta_2(s)\}$), and the pre-exponential factors $\{A_s\}$ of Eq. (5) are free parameters determined by the fits. When an EMO potential is used for the $a\,^3\Pi_{0^+}$ state, the well depth $\mathfrak{D}_e$ and equilibrium distance r_e are sometimes held fixed at the values determined by the *ab initio* calculations,[30] and sometimes allowed to vary, and the calculated difference $[V_s(r_\mathrm{x})-\mathfrak{D}_s]$ is the analog of the parameter A_s for the exponential potential energy functions. The number of free parameters in a given fit is denoted by N_p.

1. Representation for the $t\,^3\Sigma_1^+$ state potential

Mulliken's work suggested that the $t\,^3\Sigma_1^+$ state, which dissociates to the upper (I*) limit, was responsible for the continuum part of the B-band. His prediction that the potential curve for that state lay at significantly higher energy that did those for the three states giving rise to the A-band ($A\,^1\Pi_1$, $a\,^3\Pi_{0^+}$ and $a\,^3\Pi_1$) is also consistent with the intensity increase in the HI absorption continuum at frequencies above ca. 53 000 cm^{-1} observed by Romand[5,7] and by Huebert and Martin.[9] Unfortunately, the available continuum absorption coefficients do not discern the intensity maximum associated with transitions into this state, and for $\nu \gtrsim 56\,500\ \mathrm{cm}^{-1}$ their behavior is obscured by structure due to discrete absorption into various highly excited bound states.[5,7,36,37] Thus, the available data cannot provide a de-

Downloaded 07 Nov 2002 to 129.97.80.195. Redistribution subject to AIP license or copyright, see http://ojps.aip.org/jcpo/jcpcr.jsp

TABLE III. Results of fitting four final-state potentials to all data for both isotopomers. Numbers in parentheses are 95% confidence limit uncertainties yielded by the fit.

			$A\,^1\Pi$		$a\,^3\Pi_{0^+}$			$a\,^3\Pi_1$	$t\,^3\Sigma_1^+$
RMSR	$\phi_{193}(I^*)^a$	N_p	Free	A_s	Form	Free	$V_s(r_x)-\mathfrak{D}_s$	A_s	A_s
Flat transition moment functions for all four states									
1.89	0.47	12	β_0	22 143 (150)	exp	β_0	10 461 (190)	16 940 (1100)	26 479 (760)
1.87	0.46	13	β_0,β_1	22 403 (300)	exp	β_0	10 510 (200)	17 400 (1400)	26 842 (870)
1.54	0.38	13	β_0	22 951 (200)	exp	β_0,β_1	10 461 (140)	17 880 (700)	28 604 (1000)
1.44	0.40	14	β_0,β_1	22 528 (260)	exp	β_0,β_1	10 371 (110)	17 090 (1100)	28 506 (880)
1.65	0.44	11	β_0	22 521 (160)	EMO	β_0	11 173 (117)	17 373 (780)	27 458 (810)
1.65	0.43	12	β_0,β_1	22 616 (290)	EMO	β_0	11 180 (132)	17 518 (1 100)	27 585 (870)
1.61	0.43	12	β_0	22 569 (150)	EMO	β_0,β_1	11 035 (150)	17 325 (730)	27 605 (810)
1.63	0.43	12	β_0	22 557 (160)	EMO	β_0,r_e	11 091 (632)	17 526 (780)	27 513 (820)
1.52	0.40	13	β_0	22 885 (180)	EMO	$\beta_0,r_e,\ \mathfrak{D}_e$	12 710 (9384)	17 753 (620)	28 493 (950)
Transition moment functions linear in $y_4(r)$ for the first three states									**Flat TMF**
0.85	0.12	16	β_0	21 400 (530)	exp	β_0,β_1	10 959 (180)	18 215 (580)	46 250 (8 900)
0.80	0.15	16	β_0,β_1	19 900 (290)	exp	β_0	10 854 (420)	13 865 (340)	64 020 (1 600)
0.77	0.13	17	β_0,β_1	20 030 (280)	exp	β_0,β_1	10 835 (410)	13 994 (450)	58 160 (14 000)
0.91	0.11	14	β_0	19 692 (280)	EMO	β_0	11 748 (410)	13 299 (930)	110 200 (52 000)
0.94	0.11	15	β_0	19 639 (310)	EMO	β_0,β_1	11 953 (480)	13 658 (1 100)	115 410 (59 000)
0.76	0.12	15	β_0,β_1	20 063 (220)	EMO	β_0	11 420 (303)	14 013 (410)	60 750 (14 000)
0.76	0.12	16	β_0,β_1	20 080 (230)	EMO	β_0,β_1	11 355 (365)	14 009 (440)	59 480 (13 000)
Scaled *ab initio* transition moment functions for all four states									
1.57	0.23	12	β_0	20 078 (300)	exp	β_0	11 797 (190)	15 150 (1 00)	26 650 (870)
1.21	0.18	13	β_0,β_1	20 808 (220)	exp	β_0	11 301 (150)	15 758 (600)	25 230 (1 500)
0.94	0.10	13	β_0	21 071 (150)	exp	β_0,β_1	11 053 (75)	15 518 (310)	27 260 (2 100)
0.92	**0.11**	**14**	β_0,β_1	**21 136** (170)	**exp**	β_0,β_1	**11 010** (78)	**15 668** (370)	**27 450** (2 100)
1.29	0.20	11	β_0	20 425 (280)	EMO	β_0	12 285 (92)	15 511 (720)	23 800 (1 100)
1.17	0.17	12	β_0	20 630 (180)	EMO	β_0,β_1	11 916 (118)	15 214 (470)	23 850 (950)
1.08	0.16	12	β_0,β_1	21 145 (250)	EMO	β_0	12 060 (90)	16 309 (520)	27 910 (2 500)
0.94	0.15	13	β_0,β_1	21 079 (170)	EMO	β_0,β_1	11 690 (94)	15 774 (400)	25 840 (1 400)
0.90	**0.12**	**14**	β_0,β_1	**21 161** (160)	**EMO**	β_0,β_1,β_2	**11 642** (78)	**15 714** (360)	**26 890** (1 800)

[a]cf. experimental values 0.11(±0.03) and 0.09(±0.05).

finitive estimate of the position and slope of this potential function in the region of good Franck-Condon overlap with the ground-state $v=0$ level. At the same time, both Romand's results and perturbations in the discrete spectra of transitions into the highly excited $b\,^3\Pi$ states do suggest that the potential curve of the state giving rise to the red wing of the B-absorption band lies ca. $57\,000-65\,000\ \mathrm{cm}^{-1}$ above the ground-state potential minimum (or $23\,600-31\,600\ \mathrm{cm}^{-1}$ above its asymptote) at $r_x=1.609$ Å $\approx r_e(X\,^1\Sigma^+)$.

The potential form used to represent the $t\,^3\Sigma_1^+$ state is the exponential function of Eq. (5). However, since only the red tail of the t-state spectrum is observed, reflection-method arguments indicate that the slopes of the potential energy and the transition moment functions in the Franck-Condon region would be totally correlated to the strength c_0 of the transition moment and the energy of the potential A_s. In other words, the effect of changes in β_0 or c_1 on the predicted low-frequency tail of the t-state spectrum could be completely compensated for by correlated changes in A_s and c_0; numerical experiments confirmed this assertion. Thus, one can at best expect our empirical analysis to be able to determine one potential-function parameter and one transition-moment function parameter for this state.

In view of the above, the recent *ab initio* results of Alekseyev *et al.*[30] were used to provide a constraint on the shape of the $t\,^3\Sigma_1^+$ potential energy curve. An unpublished extension of their Fig. 1,[51] shows that at our expansion center, $r_x=1.609$ Å, the diabatic extension of their calculated $t\,^3\Sigma_1^+$ state potential has an energy of approximately 61 800 cm^{-1} and slope of ca. $-73\,900\ \mathrm{cm}^{-1}\ \text{Å}^{-1}$. Relative to the potential asymptote at $\mathfrak{D}_s=33\,381\ \mathrm{cm}^{-1}$, for the exponential potential form of Eq. (5) this implies that the leading potential shape parameter [the exponent coefficient in Eq. (5)] is

$$\beta_0(t\,^3\Sigma_1^+)=-V'(r_x)/[V(r_x)-\mathfrak{D}_s]$$
$$=-V''(r_x)/V'(r_x)\approx 2.6\quad \text{Å}^{-1}, \tag{10}$$

where primes ($'$) denote differentiation with respect to r. In all of the four-final-state fits described below, the exponent coefficient β_0 for the $t\,^3\Sigma_1^+$-state potential was held fixed at this value.

2. Results using constant ("flat") transition moment functions

The uppermost segment of Table III summarizes the results of fits to models based on four final-state potentials, in which all transition moment functions (TMF's) were treated as constants. The potential functions for the $A\,^1\Pi_1$, $a\,^3\Pi_1$, and $t\,^3\Sigma_1^+$ states were always represented by the exponential form of Eq. (5) in these fits. For the $a\,^3\Pi_{0^+}$ electronic state, the choice of potential function form is listed in the table

Downloaded 07 Nov 2002 to 129.97.80.195. Redistribution subject to AIP license or copyright, see http://ojps.aip.org/jcpo/jcpcr.jsp

(exponential or "exp" versus EMO), and for both it and the $A\,^1\Pi_1$ state, the potential shape parameters varied in the fit are identified in the columns labeled "free." When the $a\,^3\Pi_{0^+}$ state was represented by an exponential function, the energy parameter $A_s=[V_s(r_x)-\mathfrak{D}_s]$ was also a fitting parameter, while when an EMO potential was used for this state, the value of and uncertainty in $[V_s(r_x)-\mathfrak{D}_s]$ were calculated from those for the other fitting parameters (β_0, and when appropriate, one or more of β_1, β_2, r_e and $\mathfrak{D}_e$).

The first four rows in Table III describe cases in which all four final-state potentials were represented by exponential functions. In the first one, all exponent coefficients were treated as constants, while in the next three, one or both of the exponent parameters for the $A^1\Pi$ and $a\,^3\Pi_{0^+}$ states were allowed to be linear functions of $y_8(r)$. These results show that within this flat-TMF model, introducing that additional flexibility into the shape of the $A\,^1\Pi_1$ state potential has little effect on the overall quality of fit (represented by RMSR). On the other hand, allowing the $a\,^3\Pi_{0^+}$ potential exponent parameter to vary with r (rows 3 and 4) does yield a distinct improvement in the value of RMSR. The fact that the fitted values of the linear expansion coefficient for those two cases $[\beta_1(a\,^3\Pi_{0^+})=1.21(\pm0.17)$ and $1.57(\pm0.17)$ Å^{-1}, respectively] are large and positive suggests that within the constraint of a purely repulsive exponential form, the fit is attempting to make the $a\,^3\Pi_{0^+}$ state potential drop off increasingly sharply at larger distances, as if to mimic the presence of a potential well lying beyond the Franck-Condon overlap region.

Rows 5–9 of Table III show the results of fits in which the potential for the $a\,^3\Pi_{0^+}$ state was represented by the EMO function of Eq. (7). The results in rows 5 and 6 again confirm that within a flat-TMF model, introducing additional flexibility into the shape of the $A\,^1\Pi_1$ state potential does not improve the quality of fit. For these two cases, both r_e and $\mathfrak{D}_e$ for the EMO potential were held fixed at the *ab initio* values,[30] and only its leading exponent coefficient β_0 was allowed to vary. In the next three cases (rows 7–9), one or more of r_e, $\mathfrak{D}_e$ and β_1 was also allowed to vary. Since the predicted potential well for this state[30] lies well outside the Franck-Condon overlap region, the photodissociation data are not expected to be directly sensitive to its properties, and allowing r_e and/or $\mathfrak{D}_e$ to vary in the fits mainly serves as an indirect way of modifying the shape of the $a\,^3\Pi_{0^+}$ state potential wall in the Franck-Condon region. Freeing one or both of β_1 and r_e yields little improvement (within this flat–TMF model), and while a slightly smaller RMSR was obtained when $\mathfrak{D}_e$ was also allowed to vary, the fact that the resulting fitted value of $\mathfrak{D}_e$ is an implausible 3.7 times larger than the *ab initio* prediction[30] underlines the fact that varying the potential well parameters is merely an indirect way of adjusting the shape of the potential wall in the Franck-Condon region, and that no meaningful estimate for them can be obtained from the present analysis. Hence, in all further fits using an EMO potential for the $a\,^3\Pi_{0^+}$ state, $\mathfrak{D}_e$ and r_e were held fixed at the *ab initio* values (600 cm^{-1} and 2.7 Å, respectively).[30]

Overall, these results suggest that the data are sensitive to the fact that the $a\,^3\Pi_{0^+}$–state potential has a shallow well lying somewhat outside the Franck-Condon region. However, the quality of agreement with experiment for even the best of these flat-TMF fits is somewhat unsatisfactory, both because the overall RMSR values are distinctly larger than unity, and because of a complete inability to adequately represent the high frequency behavior of the experimental ϕ(I*) values for HI. The latter problem is clearly illustrated by the second-lowest panel of Fig. 5, which presents the results of the flat-TMF fit associated with the fourth row of Table III. The analogous plots for the other flat-TMF fits are very similar to this; in all cases, the high-frequency ϕ(I*) values calculated from the fitted potentials and TMF's pass through a minimum value of ca. $0.22-0.26$ around $48\,000-49\,000$ cm^{-1}, and increase sharply at higher frequencies.

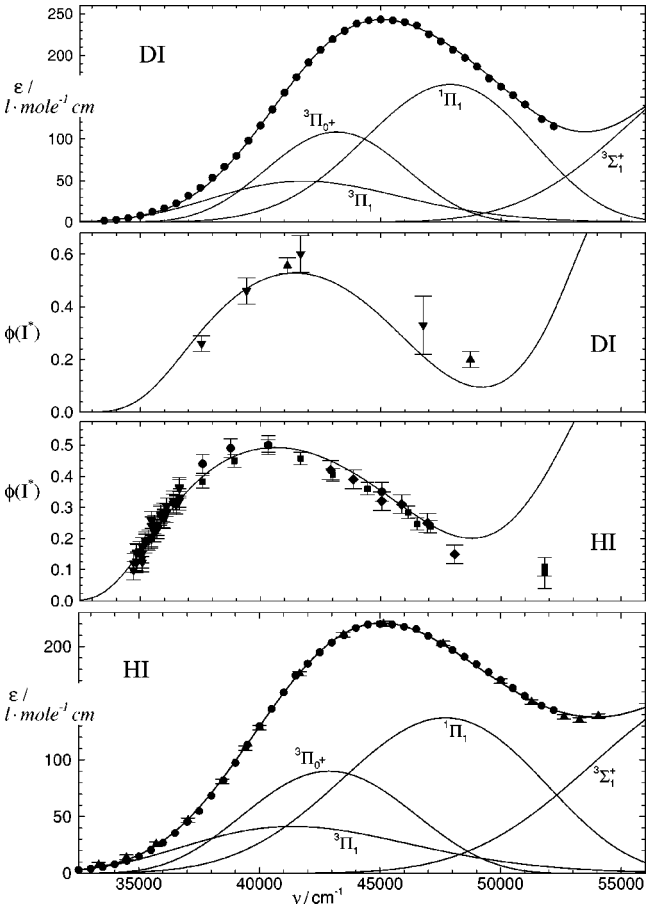

FIG. 5. Comparison with experiment (points) of results from a model using flat TMF's and exponential potentials for all four states, with linear-in-$y_8(r)$ exponent coefficients for the $A\,^1\Pi_1$ and $a\,^3\Pi_{0^+}$ states. Symbols identified as in Fig. 1.

As the (in)ability to represent the experimental ϕ(I*) values for HI at high energies seems to be a key discriminating feature in the analysis, the calculated value of ϕ(I*) at the wavelength 193 nm (energy 51 813 cm^{-1}) of the highest-energy experimental data is listed in the second column of Table III, as a second measure of the quality of fit for each case. The values of ϕ_{193}(I*) yielded by all of these flat–TMF fits are clearly much larger than the experimental values of $0.11(\pm0.03)$ and $0.09(\pm0.05)$.[21,24] Moreover, in all of these cases there is a tendency for the calculated DI total absorption coefficients to lie above the experimental values

Downloaded 07 Nov 2002 to 129.97.80.195. Redistribution subject to AIP license or copyright, see http://ojps.aip.org/jcpo/jcpcr.jsp

for the highest frequencies, as seen in the uppermost segment of Fig. 5. Although the latter discrepancies are almost within the range of realistic experimental uncertainties, they do also suggest a flat-TMF model is inadequate for explaining the experimental results at the higher frequencies.

3. Results with transition moment functions linear in $y_p(r)$

It is well documented, both here and elsewhere,[38] that it is virtually impossible to determine the r-dependence of a TMF solely from total absorption coefficients originating in the $v=0$ initial-state level, because of the very high correlation between the slope of the TMF and the position of the final-state potential. However, when the quantum yield data were included in our combined-isotopomer analysis, this limitation was removed. This conclusion is documented in the second segment of Table III by the results of fits in which the transition moment functions for the $A\,^1\Pi_1$, $a\,^3\Pi_{0^+}$, and $a\,^3\Pi_1$ states were treated as linear functions of $y_p(r)$, where for consistency with the models for the potential energy function, we again set $p=8$. Because the interparameter correlation problems discussed earlier, the transition moment function for the $t\,^3\Sigma_1^+$ state was again treated as a constant in this second group of fits.

The overall quality of fit for these linear-in-$y_8(r)$ TMF function cases is a factor of 2 better than those for the corresponding flat–TMF fits. On average, all of the experimental data are represented within the estimated experimental uncertainties (RMSR$\lesssim$1), and the associated high-frequency behavior of ϕ(I*) is generally in good agreement with experiment [see the ϕ_{193}(I*) values in column #2)]. Moreover, to within the uncertainties, the essential features of the potentials and TMF's obtained from the very best of these fits (cf. rows 12 and 16 in Table III) are the same, independent of the choice of analytic function used for the $a\,^3\Pi_{0^+}$ state potential. With regard to the TMF functions, this similarity is illustrated in Fig. 6 where the long-dash curves show the TMF's obtained from the ''exp'' case of row 12 and the dot-dash curves those for the EMO case of row 16.

From the viewpoint of a purely empirical analysis, the present study would now seem to be complete. A straightforward empirical analysis has explained all available experimental data within their uncertainties (on average) in terms of a model which attributes the spectrum to a sum of independent transitions into four final electronic states. For three of those states the analysis yields well-defined potential energy curves and r-dependent transition moment functions which in the Franck-Condon region are in semi-qualitative agreement with the recent *ab initio* results (see Fig. 6), and in the best fit of each type (rows 12 and 16 of Table III), the two sets of potentials are quite similar. On the other hand, the large variations among the A_s values for the $a\,^3\Pi_1$ and (especially!) the $t\,^3\Sigma_1^+$ state yielded by fits of fairly similar quality is somewhat troubling. Moreover, all of the fitted A_s values for the $t\,^3\Sigma_1^+$ state lie far outside the range ($23\,600 - 31\,600\ \mathrm{cm}^{-1}$) suggested by experiment, and the associated fitted TMF strength coefficients $c_0(t\,^3\Sigma_1^+)$ are more than an order of magnitude larger than the *ab initio* TMF for this

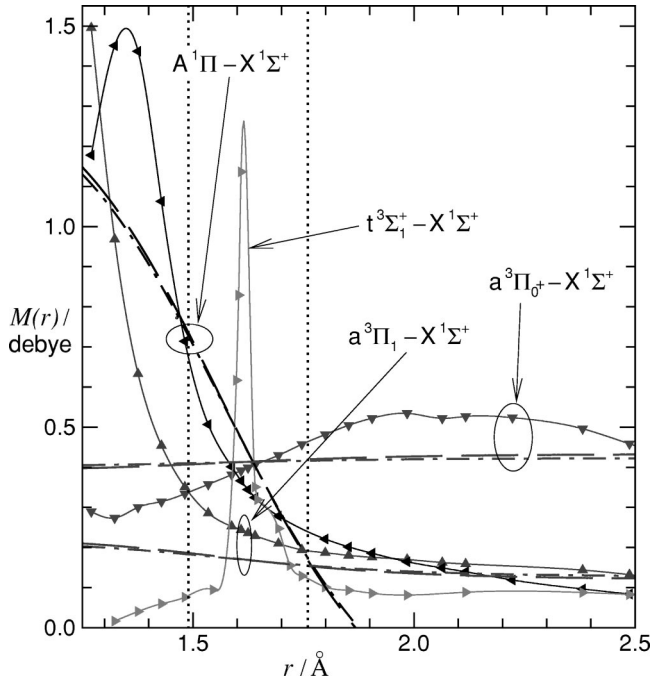

FIG. 6. Comparison of TMF functions obtained from fits using linear-in-$y_8(r)$ TMF's for the $A\,^1\Pi_1$, $a\,^3\Pi_{0^+}$, and $a\,^3\Pi_1$ states, obtained from fits using an exponential (long-dashed curves) or EMO (dot-dashed curves) potential for the $a\,^3\Pi_{0^+}$ state, with the *ab initio* values (points joined by solid curves), as scaled by the $c_0(s)$ parameters of Table IV. The vertical dotted lines indicate the approximate boundaries of the Franck-Condon overlap region, and large open circles are used to label groups of results for a given transition.

state. In addition, the scaling of the DI total absorption coefficient data required to make them consistent with those for HI, within this model, $f_\varepsilon \approx 1/0.925(\pm 0.005)$,[52] deviates from unity more than might be expected.

The main source of these difficulties is almost certainly the fact that the transition moment function for the $t\,^3\Sigma_1^+$ state was treated as a constant, a constraint imposed by interparameter correlation and the fact that only the red wing of the spectrum for this state is within the range of the existing data. This flat-TMF approximation is very strongly contradicted by the theoretical prediction of a TMF for this state which has a very sharp spike in the middle of the Franck-Condon region (see Fig. 6).[30,51] This suggests that the physical significance of an analysis which ignores the strong r-dependence of this transition moment function is questionable. In order to obtain the most realistic possible physical model for this system, we therefore chose to utilize the *ab initio* transition moment functions of Ref. 30.

4. Results using the ab initio transition moment functions

As was mentioned earlier, a particularly interesting feature of the *ab initio* calculations of Ref. 30 was their prediction of strongly r-dependent transition moment functions for the electronic transitions giving rise to the UV photodissociation spectrum of HI. Their results for the four transitions of interest, scaled slightly as described below, are plotted in Fig. 6 (points joined by solid curves). For the $A\,^1\Pi_1$,

Downloaded 07 Nov 2002 to 129.97.80.195. Redistribution subject to AIP license or copyright, see http://ojps.aip.org/jcpo/jcpcr.jsp

$a\,^3\Pi_{0^+}$, and $a\,^3\Pi_1$ states, these are the results reported in Table V of Ref. 30; for the $t\,^3\Sigma_1^+$ state, however, they are modified function values calculated by Alekseyev[51] which correspond to an ''effective diabatic'' description of that state. For the first three of these functions, Fig. 6 shows that the slope and strengths of these *ab initio* TMF's (points joined by solid curves) in the Franck-Condon region are roughly similar to those of the empirical linear-in-$y_8(r)$ functions determined above (long-dash and dot-dashed curves). However, it is also clear that they do not represent the shape of those *ab initio* functions adequately, even in that narrow region, and the (constant) fitted $t\,^3\Sigma_1^+$ state values have magnitudes of several debye, which is completely unrelated to the strength of the narrow peaked function calculated by Alekseyev.[51]

The final segment of Table III summarizes the results of fits in which each of the four transition moment functions was defined by a cubic spline function through the *ab initio* TMF values,[30,51] $\mathbb{M}_s(r)$, multiplied by a fitted scaling factor, while the potentials were represented in the same manner as in the preceding sets of fits. The overall quality of fit for these cases was not quite as good as those for the analogous purely empirical TMF-linear-in-$y_8(r)$ fits. However: (i) There is good agreement among the fitted A_s [or $V_s(r_x) - \mathfrak{D}_s$] values for most of these cases, (ii) the A_s values determined for the $t\,^3\Sigma_1^+$ state are always within the range suggested by experiment, and (iii) the associated fitted values of the DI absorption coefficient scaling factor $f_\varepsilon \approx 1/0.965$ (± 0.007) is relatively close to unity.[52] The model *in*dependence of these results indicates that in spite of the slightly larger RMSR values, this model is physically more realistic than is the purely empirical analysis in which the TMF for the $t\,^3\Sigma_1^+$ state had to be treated as a constant and the others as simple linear functions of $y_8(r)$. Moreover, the best of these scaled-theoretical-TMF fits still explains all of the data to well within the experimental uncertainties.

Consideration of the values of $\phi_{193}(\mathrm{I}^*)$ yielded by these scaled-theoretical-TMF fits clearly delineates which cases yield the most realistic results; the two optimum cases are identified by bold-font entries in Table III. Note that these two fits have the same total number of free parameters (N_p), and more particularly, although they involve different functional forms for the $a\,^3\Pi_{0^+}$ state potential, both require the same number of free potential parameters to describe that state. The potential curves obtained for these two cases are compared in Fig. 7; it is clear that the choice of functional form for the $a\,^3\Pi_{0^+}$ potential has no significant effect on the nature of the resulting potential functions in the Franck-Condon overlap region. These two (''bold-font'') cases provide essentially equivalent representations of the experimental data, and yield potential energy functions which are essentially equivalent in the Franck-Condon region. However, although the data considered here are not sensitive to its properties, the fact that theory predicts that the $a\,^3\Pi_{0^+}$ state has a shallow well around 2.7 Å leads us to select the model in which the EMO potential form was used for this state (last row in Table III) as our final recommended result. The excellent agreement of this model with the experimental data used in the analysis is seen in Fig. 8.

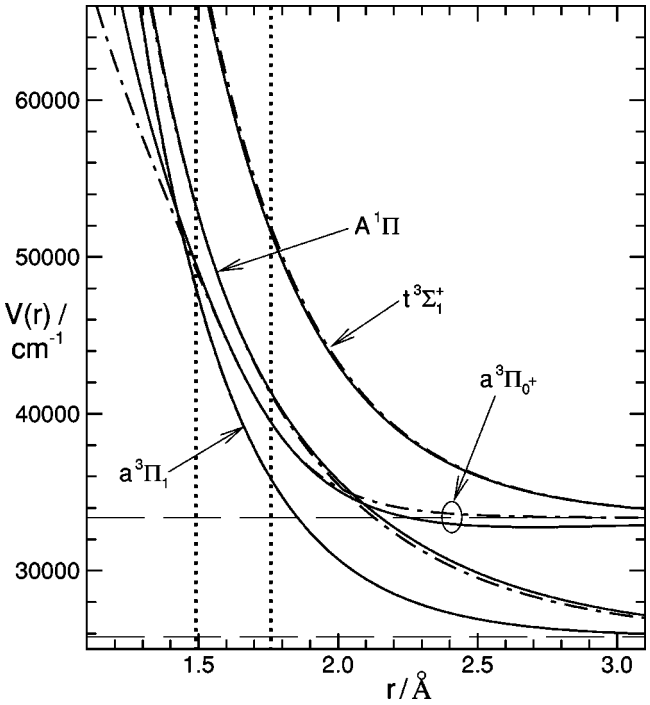

FIG. 7. Comparison of final-state potential functions obtained from fits using scaled *ab initio* TMF's for all four transitions, an exponential with a linear-in-$y_8(r)$ exponent coefficient for the $A\,^1\Pi_1$ state potential, and either an EMO function with quadratic-in-$y_8(r)$ exponent coefficient (solid curves) or an exponential with a linear-in-$y_8(r)$ exponent coefficient (dot-dashed curves) for the $a\,^3\Pi_{0^+}$ state potential (bold font cases in Table III). The vertical dotted lines indicate the approximate boundaries of the Franck-Condon overlap region, and the large open circle facilitates labeling different estimates of the $a\,^3\Pi_0^+$ potential curve.

As an independent test of the validity of our recommended model, it was used to predict and compare with experiment values of the parameter characterizing the anisotropy of the distribution of photofragment I* atoms. For the parallel transition $a\,^3\Pi_{0^+} \leftarrow X\,^1\Sigma^+$ this parameter has the value $+2$, while for the perpendicular transition $t\,^3\Sigma_1^+ \leftarrow X\,^1\Sigma^+$ it is -1, so the quantity calculated from the various partial absorption coefficients is

$$\beta(\mathrm{I}^*) = \frac{2\,\epsilon(\nu,\mathrm{T};\,a\,^3\Pi_{0^+}) - \epsilon(\nu,\mathrm{T};\,t\,^3\Sigma_1^+)}{\epsilon(\nu,\mathrm{T};\,a\,^3\Pi_{0^+}) + \epsilon(\nu,\mathrm{T};\,t\,^3\Sigma_1^+)}. \tag{11}$$

The excellent agreement of our predictions with the experimental values of Gendron and Hepburn[26] and of Langford *et al.*[25] seen in Fig. 9 provides further assurance of the validity of the present results. Figures 8 and 9 suggest that measurements of the quantum yield and the I* photofragment anisotropy distribution at frequencies $\gtrsim 50\,000$ cm^{-1} would provide a discerning test of the present description of this system.

The parameters defining this final recommended set of potential energy functions and the associated (fitted) TMF scaling parameters are listed in Table IV. The numbers of significant digits required to adequately represent the various fitted parameters were minimized using the sequential rounding and refitting procedure of Ref. 53, which is implemented in program BCONT.[46] We note that our conclusion that the DI absorption coefficients should all be increased by ca. 3.2%

Downloaded 07 Nov 2002 to 129.97.80.195. Redistribution subject to AIP license or copyright, see http://ojps.aip.org/jcpo/jcpcr.jsp

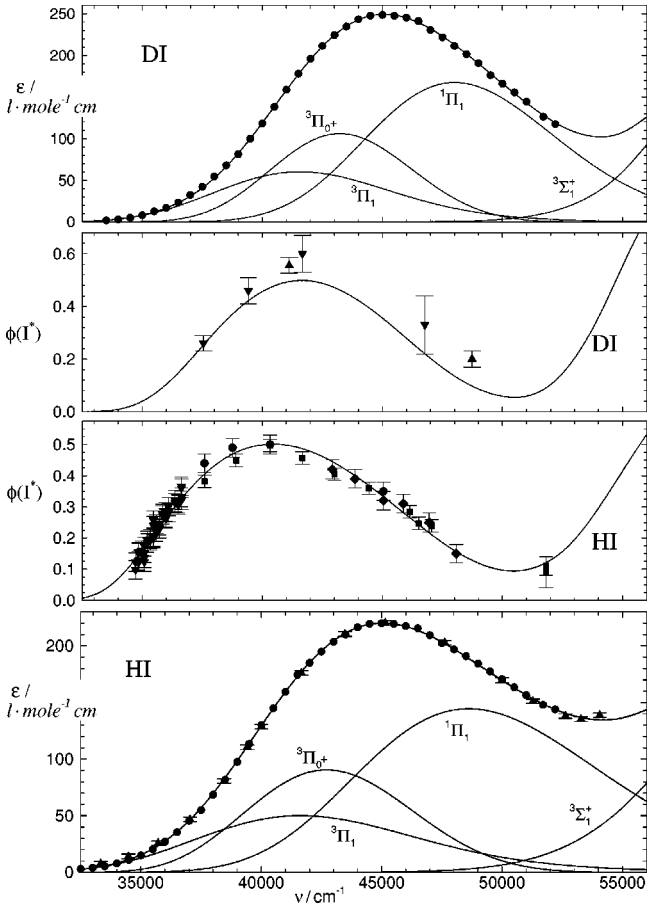

FIG. 8. Comparison with experiment (points) of results of the fit using the recommended model of Table IV, which uses scaled *ab initio* TMF's for all four states, an exponential with a linear-in-$y_8(r)$ exponent coefficient for the $A\,^1\Pi_1$ state potential, and an EMO function with a quadratic-in-$y_8(r)$ exponent coefficient for the $a\,^3\Pi_{0^+}$ state potential. Symbols identified as in Fig. 1.

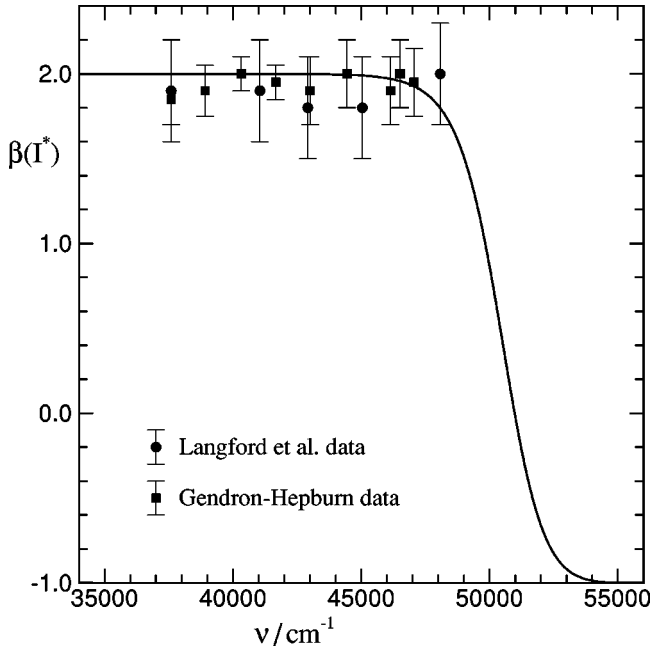

FIG. 9. Comparison with experiment (Refs. 25, 26) of I* photofragment anisotropy distribution parameters calculated from the final recommended model of Table IV.

[since[52] $f_\varepsilon = 0.9694(\pm 0.0047)$] is well within Ogilvie's estimated absolute uncertainty of 5%. Note too that this is a relative correction factor, and the truth might be that the HI absorption coefficients are 3.1% too large, rather than the DI values being 3.1% too small, or some intermediate combination of scaling factors. As mentioned earlier, Ogilvie's 5% absolute (pressure measurement) uncertainty[10] implies an overall uncertainty of 2.5% in the strength of our final recommended TMF's for this system.

Finally, since this analysis involves TMF's defined as spline functions through the *ab initio* function values, multiplied by an empirical fitting parameter, for the convenience of potential users, Table V lists the resulting final scaled set of TMF function values. Cubic spline functions through those sets of points define our final recommended TMF functions. It is reassuring to note (last row of Table IV) that the fitted TMF scaling factors are generally close to unity; this attests both to the high quality of the original *ab initio* TMF values of Alekseyev *et al.*[30,51] and to the physical significance of the present results. As mentioned earlier, the computer program used in this analysis may be freely downloaded from the first author's www site (http://leroy.uwaterloo.ca), while the input data file for the final fit, including all of the experimental data used in this analysis, may be obtained from the Journal's online archive.[54] In addition, tables of partial and total absorption coefficients for HI and DI calculated for a wide range of frequencies at temperatures T=10, 300 and 1000 K are included with the archived data.[54]

V. DISCUSSION AND CONCLUSIONS

The potential energy and transition moment functions presented in Tables IV and V represent our current best understanding of the UV photodissociation spectra of HI and DI. These functions are able to account for all of the available absorption coefficient and quantum yield data within the estimated experimental uncertainties (on average), without any need to invoke the type of coupling amongst various final-state continuum wave functions proposed by Levy and Shapiro.[35] Thus, while such coupling certainly may occur, we find no empirical evidence that it contributes to the existing HI and DI photodissociation spectra.

It is interesting to note that the above conclusion is very different from that reported by Alexander *et al.*[55] and Regan *et al.*[56] for the analogous UV photodissociation of HCl. They concluded that the absorption step excites HCl into the $A\,^1\Pi$ state, and that non-Born-Oppenheimer coupling between it and the neighboring triplet states at distances well outside the Franck-Condon overlap region governed the production of spin–orbit excited Cl* atoms. If such interstate coupling were occurring for HI, we would expect to find our independent-state analysis unable to explain the observed branching ratios. Had we considered only constant TMF's in our analysis, this would have appeared to be the case (see Fig. 5). However, Fig. 8 shows that an independent-state analysis using r-dependent TMF's is able to account for all

Downloaded 07 Nov 2002 to 129.97.80.195. Redistribution subject to AIP license or copyright, see http://ojps.aip.org/jcpo/jcpcr.jsp

TABLE IV. Parameters defining the recommended final-state potential energy and transition moment functions for HI and DI (with 95% confidence limit uncertainties in parentheses) where the potential function exponent coefficients expansion variable is $y_8(r)$, and the fit yields $f_\epsilon(\mathrm{DI}) = 1/0.9694(\pm 0.0047)$ (Ref. 52).

	$A\,^1\Pi_1$	$a\,^3\Pi_{0^+}$	$a\,^3\Pi_1$	$t\,^3\Sigma_1^+$
$\mathfrak{D}_s/\mathrm{cm}^{-1}$	25 778	33 381	25 778	33 381
g_u	2	1	2	2
Potential energy function parameters				
form	expt	EMO	expt	expt
A_s/cm^{-1}	21 161 ($\pm$160)	a	15 714 ($\pm$360)	26 890 ($\pm$1 800))
$\beta_0/\mathrm{Å}^{-1}$	2.128 ($\pm$0.048)	1.546 59 ($\pm$0.0025)	2.949 ($\pm$0.091)	2.60 ($---$)
$\beta_1/\mathrm{Å}^{-1}$	$-$0.30 ($\pm$0.12)	0.067 ($\pm$0.011)	$---$	$---$
$\beta_2/\mathrm{Å}^{-1}$	$---$	$-$0.074 ($\pm$0.022)	$---$	$---$
Parameters scaling the ab initio transition moment functions				
c_0	0.9368 ($\pm$0.027)	1.014 ($\pm$0.014)	1.468 ($\pm$0.12)	0.93 ($\pm$0.38)

[a]EMO potential form with fixed $\mathfrak{D}_e = 600\ \mathrm{cm}^{-1}$ and $r_e = 2.7$ Å implies $V_s(r_x) - \mathfrak{D}_s = 11\,642(\pm 78)\ \mathrm{cm}^{-1}$.

available data, which suggests that such coupling is not important for HI. This conclusion is supported by a recent time-dependent wave packet simulation of HI photolysis using the potential curves and transition moment functions of Ref. 30 together with a new theoretical spin-rotational matrix element coupling the $A\,^1\Pi_1$ and $a\,^3\Pi_{0^+}$ states, which found that spin-rotational coupling had no significant effect on the predicted spectrum.[57]

This is the first empirical analysis of this system since the early work of Romand[7] to take quantitative account of the observed part of the UV B-band which begins to dominate this spectrum at frequencies above 50 000 cm^{-1}. The fact that the existing data only sample the tail of the red wing of this spectrum means that a definitive description of this state cannot be obtained here. However, it is reassuring to note the good agreement between the energy of this state in the middle of the Franck-Condon region determined here ($A_s + 33\,381 = 60\,271(\pm 1800)\ \mathrm{cm}^{-1}$) with the energy 61 800 cm^{-1} associated with the effective diabatic potential of Alekseyev *et al.*[30,51]

TABLE V. *Ab initio* transition moment function values coupling the $X\,^1\Sigma^+$ state of HI to various excited states (Refs. 30, 51), converted to debye units and scaled by the factors listed in Table IV.

r/a.u.	$A\,^1\Pi$	$a\,^3\Pi_{0^+}$	$a\,^3\Pi_1$	$t\,^3\Sigma_1^+$
2.40	1.178 054	0.289 228	1.495 388	⋯
2.50	1.450 882	0.273 558	0.968 717	0.016 547
2.60	1.437 048	0.300 285	0.632 752	0.040 421
2.70	1.063 023	0.314 306	0.454 060	0.059 805
2.80	0.714 095	0.333 894	0.350 741	0.076 115
2.90	0.506 676	0.357 347	0.285 742	⋯
2.92	⋯	⋯	⋯	0.094 553
3.00	0.401 217	0.381 471	0.252 757	⋯
3.02	⋯	⋯	⋯	0.616 675
3.03	⋯	⋯	⋯	0.829 089
3.04	0.366 310	0.391 523	0.243 877	1.136 481
3.07	0.344 356	0.398 662	0.235 743	⋯
3.10	0.324 450	0.406 214	0.229 101	0.350 697
3.11	⋯	⋯	⋯	0.319 117
3.20	0.278 328	0.429745	0.209810	0.247 327
3.25	⋯	⋯	⋯	0.155 209
3.30	⋯	0.457 219	0.194 214	0.128 876
3.40	0.221 062	0.481 704	0.186 900	0.101 408
3.50	0.201 442	0.504 719	0.180 370	0.093 111
3.60	0.185 703	0.522 348	0.175 557	0.085 760
3.75	0.164 511	0.534 436	0.170 109	0.081 363
3.90	0.149 058	0.522 013	0.162 460	⋯
4.00	0.139 438	0.526 730	0.158 916	0.088 454
4.20	0.118 960	0.523 663	⋯	⋯
4.50	0.096 483	0.495 982	0.143 655	0.087 816
4.70	0.084 053	0.458 533	0.132 274	0.082 828
4.80	0.078 791	0.439 951	0.125 035	⋯
5.00	0.070 719	0.396 394	0.109 327	0.072 948

Comparisons of the present potentials (solid curves) both with the *ab initio* potentials (points) and with the sets of final-state potentials reported by Clear *et al.*[16] (dashed curves) and by Gendron and Hepburn[26] (dot-dot-dashed curves) are presented in Fig. 10. Those earlier analyses focussed attention on the lower-frequency A-band region, and made no attempt to characterize the $t\,^3\Sigma^+$ state. The Gendron-Hepburn analysis neglected both the data for the second isotopomer (DI) and the r-dependence of the transition moment function, while the Clear *et al.*[16] analysis made only the latter approximation. Thus, it seems clear that the availability of data for more than one (small reduced mass) isotopomer is very important for allowing a unique multi-state deconvolution of featureless absorption spectra such as those seen in the top and bottom segments of Fig. 1.

One key feature of this analysis is the determination that although essentially all of the photodissociation data involves transitions originating in the $v = 0$ vibrational level of the initial state, those data could not be adequately described without taking account of the r-dependence of the TMF's. This is partly due to the presence of data for more than one isotopomer, and partly because of the inclusion of the quantum yield data in the analysis. It is clear from Fig. 6 that the empirical [linear in $y_8(r)$] TMF's determined in the analysis described above (dashed and dot-dashed-curves) do not agree well with the shapes of the recent *ab initio* results of Alekseyev *et al.*[30] (points and solid curves); at the same time, those *ab initio* TMF's cannot fully account for the experimental data without the modest scaling determined by the present analysis. It is also clear than no empirical analy-

Downloaded 07 Nov 2002 to 129.97.80.195. Redistribution subject to AIP license or copyright, see http://ojps.aip.org/jcpo/jcpcr.jsp

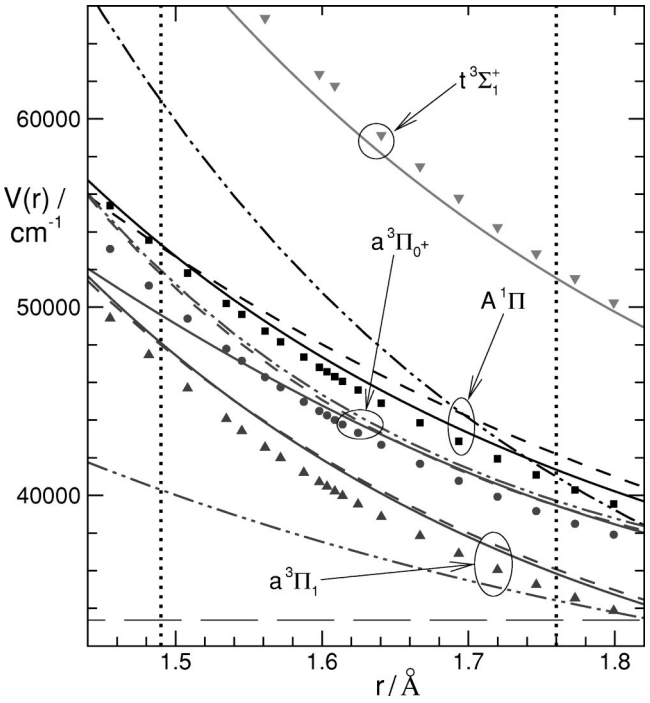

FIG. 10. Comparison of the present recommended final-state potential functions of Table IV (solid curves) with the *ab initio* potentials functions (Refs. 30, 51; points), and with the sets of three final-state potentials reported by Gendron and Hepburn (Ref. 26) (dot-dot-dashed curves) and by Clear *et al.* (Ref. 16) (short-dash curves). The vertical dotted lines indicate the approximate boundaries of the Franck-Condon overlap region, and the large open circles facilitate labeling different estimates of a given potential curve.

sis is likely to be able to determine accurately a TMF with the unusual shape associated with the theoretical function for the $t\,^3\Sigma_1^+ \rightarrow X\,^1\Sigma^+$ transition. Thus, our recommended TMF's for this system are spline functions through the (scaled) *ab initio* points of Table V.

Finally, it appears that after more that a century of study we have finally attained a definitive description of the UV photodissociation spectrum of HI and DI in the lower-frequency A-band region, and a good semiquantitative description of the portion of the B-band accessed by current experiments. The resulting potentials and transition moment functions allow us to readily generate reliable predictions of total and partial absorption coefficients and of photodissociation branching ratios for this system across this whole region.[54] This study illustrates the utility of incorporating total absorption coefficient and quantum yield (or branching ratio) data in the same analysis, and the importance of having good total absorption coefficient data over a wide frequency range for more than one isotopomer of such small-reduced-mass systems.

ACKNOWLEDGMENTS

The authors are pleased to acknowledge helpful discussions with Professor J. W. Hepburn and Professor H.-P. Loock and Dr. G. J. Gendron and Dr. A. Brown, and we particularly wish to thank Dr. A. B. Alekseyev for insightful correspondence and for providing us with his unpublished predictions of the effective diabatic $t\,^3\Sigma_1^+ - X\,^1\Sigma^+$ transition moment function.

[1] Lemoine, Ann. Chim. Phys. **12**, 145 (1877).
[2] G. K. Rollefson and J. E. Booher, J. Am. Chem. Soc. **53**, 1728 (1931).
[3] J. R. Bates, J. O. Halford, and L. C. Anderson, J. Chem. Phys. **3**, 415 (1935).
[4] C. F. Goodeve and A. W. C. Taylor, Proc. R. Soc. London, Ser. A **A 154**, 181 (1936).
[5] J. Romand and B. Vodar, Compt. Rend. **226**, 890 (1948).
[6] J. Romand, Compt. Rend. **227**, 117 (1948).
[7] J. Romand, Ann. Phys. (Paris) **A 4**, 527 (1948).
[8] R. E. Martin and J. E. Willard, J. Chem. Phys. **40**, 2999 (1964).
[9] B. J. Huebert and R. M. Martin, J. Phys. Chem. **72**, 3046 (1968).
[10] J. F. Ogilvie, Trans. Faraday Soc. **67**, 2205 (1971).
[11] R. J. Donovan and D. Husain, Trans. Faraday Soc. **62**, 1050 (1966).
[12] P. Cadman and J. C. Polanyi, J. Phys. Chem. **72**, 3715 (1968).
[13] L. E. Compton and R. M. Martin, J. Phys. Chem. **73**, 3474 (1969).
[14] G. A. Oldershaw, D. A. Porter, and A. Smith, J. Chem. Soc., Faraday Trans. 1 **1 68**, 2218 (1972).
[15] J. A. Betts, Ph D. Thesis, California Institute of Technology (1972), as reported by Clear *et al.* (Ref. 16).
[16] R. D. Clear, S. J. Riley, and K. R. Wilson, J. Chem. Phys. **63**, 1340 (1975).
[17] R. Schmiedl, H. Dugan, W. Meier, and K. H. Welge, Z. Phys. A **304**, 137 (1982).
[18] Z. Xu, B. Koplitz, and C. Wittig, J. Phys. Chem. **92**, 5518 (1988).
[19] Z. Xu, B. Koplitz, and C. Wittig, J. Chem. Phys. **90**, 2692 (1989).
[20] P. Brewer, P. Das, G. Ondrey, and R. Bersohn, J. Chem. Phys. **79**, 720 (1983).
[21] C. A. Wight and S. R. Leone, J. Chem. Phys. **79**, 4823 (1983).
[22] A. J. R. Heck and D. W. Chandler, Annu. Rev. Phys. Chem. **46**, 335 (1995).
[23] L. McDonnell and A. J. R. Heck, J. Mass Spectrom. **33**, 415 (1998).
[24] G. N. A. van Veen, K. A. Mohamed, T. Baller, and A. E. de Vries, Chem. Phys. **80**, 113 (1983).
[25] S. R. Langford, P. M. Regan, A. J. Orr-Ewing, and M. N. R. Ashfold, Chem. Phys. **231**, 245 (1998).
[26] D. J. Gendron and J. W. Hepburn, J. Chem. Phys. **109**, 7205 (1998).
[27] P. M. Regan, D. Ascenzi, C. Clementi, M. R. N. Ashfold, and A. J. Orr-Ewing, Chem. Phys. Lett. **315**, 187 (1999).
[28] S. Manzhos, H.-P. Loock, B. L. G. Bakker, and D. H. Parker, J. Chem. Phys. **117**, 9347 (2002) (preceding paper).
[29] R. S. Mulliken, Phys. Rev. . **51**, 310 (1937)
[30] A. B. Alekseyev, H.-P. Liebermann, D. B. Kokh, and R. J. Buenker, J. Chem. Phys. **113**, 6174 (2000).
[31] E. U. Condon, Phys. Rev. **32**, 858 (1928).
[32] J. G. Winans and E. C. G. Stueckelberg, Proc. Natl. Acad. Sci. U.S.A. **14**, 867 (1928).
[33] J. F. Ogilvie and R. H. Tipping, Faraday Discuss. Chem. Soc. **53**, 153 (1972).
[34] J. Tellinghuisen, J. Chem. Phys. **58**, 2821 (1973).
[35] I. Levy and M. Shapiro, J. Chem. Phys. **89**, 2900 (1988).
[36] W. C. Price, Proc. R. Soc. London, Ser. A **A 167**, 216 (1938).
[37] S. G. Tilford, M. L. Ginter, and A. M. Bass, J. Mol. Spectrosc. **34**, 327 (1970).
[38] R. J. Le Roy, R. G. Macdonald, and G. Burns, J. Chem. Phys. **65**, 1485 (1976).
[39] J. Tellinghuisen, in *Photodissociation and Photoionization*, edited by K. P.Lawley (Wiley, New York, 1985), Vol. 60 of Adv. Chem. Phys., pp. 299–369.
[40] H. Lefebvre-Brion and R. W. Field, *Perturbations in the Spectra of Diatomic Molecules* (Academic, New York, 1986).
[41] E. E. Whiting, A. Schadee, J. B. Tatum, J. T. Hougen, and R. W. Nicholls, J. Mol. Spectrosc. **80**, 249 (1980).
[42] G. Herzberg, *Spectra of Diatomic Molecules* (Van Nostrand, Toronto, 1950).
[43] J. A. Coxon and P. G. Hajigeorgiou, J. Mol. Spectrosc. **150**, 1 (1991).
[44] P. G. Hajigeorgiou and R. J. Le Roy, J. Chem. Phys. **112**, 3949 (2000).
[45] E. G. Lee, J. Y. Seto, T. Hirao, P. F. Bernath, and R. J. Le Roy, J. Mol. Spectrosc. **194**, 197 (1999).
[46] R. J. Le Roy and G. T. Kraemer, *BCONT 2.0. Computer Program for Calculating Absorption Coefficients, Emission Intensities or (Golden Rule) Predissociation Rates*, University of Waterloo Chemical Physics Research Report CP-650 (2002). The source code and manual for this program may be obtained from ''Computer Programs'' link on the www site http://leroy.uwaterloo.ca

Downloaded 07 Nov 2002 to 129.97.80.195. Redistribution subject to AIP license or copyright, see http://ojps.aip.org/jcpo/jcpcr.jsp

[47] R. Brühl, J. Kapetanakis, and D. Zimmermann, J. Chem. Phys. **94**, 5865 (1991).
[48] F. Bokelmann and D. Zimmermann, J. Chem. Phys. **104**, 923 (1996).
[49] Y. Huang, "*Determining Analytical Potential Energy Functions of Diatomic Molecules by Direct Fitting*," M Sc. Thesis, Department of Chemistry, University of Waterloo (2002).
[50] For all (positive) values of p, $y_p(r)$ is approximately linear in $(r-r_x)$ when $|r-r_x|$ is small, and both the quality of fit and nature of the resulting fitted functions near r_x are essentially independent of the value chosen for p. However, for large values of $|r-r_x|$ both $y_p(r)$ and functions expressed in terms of it approach their limiting asymptotic values more rapidly when p is large.
[51] A. B. Alekseyev, private communication (2001).
[52] The scaling factor which is required to make the DI total absorption coefficients consistent with those for HI is defined as an inverse, since it is more convenient in the fits to scale the calculated intensities for a given case, than to scale a subset of the data.
[53] R. J. Le Roy, J. Mol. Spectrosc. **191**, 223 (1998).
[54] See EPAPS Document No. E-JCPSA6-117-002243 for an ASCII file comprising the input data file for program BCONT (Ref. 46) containing all of the data used in the present analysis, plus a file containing predictions of total and partial absorption coefficients for HI and DI at T=10 , 300, and 1000 K generated from the final recommended model of Table IV. A direct link to this document may be found in the online article's HTML reference section. The document may also be reached via the EPAPS homepage (http://www.aip.org/pubservs/epaps.html) or from ftp.aip.org in the directory /epaps/. See the EPAPS homepage for more information.
[55] M. H. Alexander, B. Pouilly, and T. Duhoo, J. Chem. Phys. **99**, 1752 (1993).
[56] P. M. Regan, D. Ascenzi, A. Brown, G. G. Baliut-Kurti, and A. J. Orr-Ewing, J. Chem. Phys. 10259 (2000).
[57] N. Balakrishnan, A. B. Alekseyev, and R. J. Buenker, Chem. Phys. Lett. **341**, 594 (2001).

Downloaded 07 Nov 2002 to 129.97.80.195. Redistribution subject to AIP license or copyright, see http://ojps.aip.org/jcpo/jcpcr.jsp